REVIEWS

Journal of Semiconductors
(2020) 41, 091705
doi: 10.1088/1674-4926/41/9/091705

Recent progress on nanostructured bimetallic electrocatalysts for water splitting and electroreduction of carbon dioxide

Can Cui[1], Xiaosong Hu[2], and Liaoyong Wen[2, †]

[1]Department of Materials Science and Engineering & Institute of Materials Science, University of Connecticut, Storrs, Connecticut, 06269-3136, United States of America

[2]Key Laboratory of 3D Micro/Nano Fabrication and Characterization of Zhejiang Province, School of Engineering, Westlake University, Hangzhou 310024, China

Abstract: The exploitation of renewable energy as well as the elimination of the harmful impact of excessive carbon emission are worldwide concerns for sustainable development of the ecological environment on earth. To address that, the technologies regarding energy conversion systems, such as water splitting and electroreduction of carbon dioxide, have attracted significant attention for a few decades. Yet, to date, the production of green fuels and/or high energy density chemicals like hydrogen, methane, and ethanol, are still suffering from many drawbacks including high energy consumption, low selectivity, and sluggish reaction rate. In this regard, nanostructured bimetallic materials that is capable of taking the full benefits of the coupling effects between different elements/components with structure modification in nanoscale are considered as a promising strategy for high-performance electrocatalysts. Herein, this review aims to outline the important progress of these nanostructured bimetallic electrocatalysts. It starts with the introduction of some important fundamental background knowledge about the reaction mechanism to understand how these reactions happen. Subsequently, we summarize the most recent progress regarding how the nanostructured bimetallic electrocatalysts manipulate the activity and selectivity of catalytic reactions in the order of bimetallic alloying effect, interface/substrate effect of bi-component electrocatalyst, and nanostructuring effect.

Key words: bimetallic electrocatalysts; nanostructures; water splitting; electroreduction of carbon dioxide

Citation: C Cui, X S Hu, and L Y Wen, Recent progress on nanostructured bimetallic electrocatalysts for water splitting and electroreduction of carbon dioxide[J]. *J. Semicond.*, 2020, 41(9), 091705. http://doi.org/10.1088/1674-4926/41/9/091705

1. Introduction

In the rapid development and advancement of industrial society, the issues of excessive exploitation and over-reliance on fossil fuel accelerate the depletion earth's resources, which tremendously threatens our future. Meanwhile, the over-usage of fossil fuels leads to severe environment pollution and extreme climate change jeopardizing the whole ecosystem on the earth. Hence, the concerns about sustainability and security of energy on our planet have been raised widely, which urges researchers to address these serious issues by developing versatile energy conversion technologies to store and recycle clean and renewable sources, thus, reducing the dependency on traditional fossil fuel[1, 2]. So far, primary renewable energy sources including solar and wind power are environmentally friendly but suffer from seasonal intermittent and regional variability[3]. To prevent this drawback and fully utilize these clean and renewable resources, this unstable energy can be previously converted and stored into other form of stable and high energy density fuels and chemicals[4–6], like hydrogen and hydrocarbons, by electrocatalysis.

Water splitting was the most wide-studied electrocatalysis process owing to convenience, negligible environment pollution, and huge water feedstocks. By far, however, the overall efficiency of water splitting is still obstructed, primarily, by the sluggish kinetics of the half reaction of oxygen evolution[7, 8], given the superb intrinsic activity of Pt-based electrocatalysts which nearly approach the theoretical redox potential for HER (0 V vs. RHE)[9, 10]. Meanwhile, Ir/Ru-based metal and derived metal compounds have been recognized as conventional high-performance electrocatalysts for OER in acidic media for many years due to the suitable electronic structure of surface atoms. On the other hand, in order to prevent extreme climate and natural disaster, electroreduction of carbon dioxide has also gained much attention recently due to its potential to help close the anthropogenic carbon cycle and relieve global warming[4, 11]. The conversion of CO_2 into other common carbon chemicals like carbon monoxide (CO), formic acid (HCOOH), multi-carbon oxygenates, and hydrocarbons, is highly desirable for a sustainable energy recycling system[11, 12]. Up to now, the single/poly-crystalline pure metal electrocatalysts for CO_2RR has been widely studied regarding improving selectivity and activity of CO_2RR. The traditional metal electrodes include wide range of noble metal like Au, Ag, and Pt, transition metal, e.g. Ni, Fe, Cd, Zn, and many main group elements including Tl, In, Sn, Cd, and Pb. Among these metal based electrode, Cu, due to its unique electronic properties that are capable of producing multi-carbon products with high Faradaic efficiency (FE), serve as an ideal platform for in-depth studies regarding the potential reaction mechanism, manipulation of terminal products, as well as design and fabrication of high-performance electrodes[12].

In terms of these conventional pure metal electrocataly-

Correspondence to: L Y Wen, wenliaoyong@westlake.edu.cn
Received 1 JULY 2020; Revised 13 JULY 2020.

sts, no matter which reactions they are employed to work for, most of them endure either limited source, high cost, poor stability, or low Faradaic efficiency and selectivity[8, 10, 12]. Upon a wide diversity of promising candidates, the nanostructured bimetallic electrocatalysts have emerged and quickly drawn much interest over the past decade due to their ability to dramatically improving the activity, stability, and selectivity of catalytic reactions, while reducing cost[13, 14]. These exciting enhancements are mainly attributed to the synergistic effects between different elements and/or components, as well as the introduction of novel structures in nano scale. Consequently, the surface electronic structure of electrode, the binding energy and the spillover effect of intermediates in water splitting and/or CO_2RR can be significantly adjusted and/or improved towards specific terminate products. Therefore, in this review, we aim to summarize and discuss the progress of typically nanostructured bimetallic electrocatalysts towards efficiently water splitting and CO_2 electroreduction. Firstly, the fundamental background knowledge related to the mechanism/reaction pathways for water splitting and CO_2RR will be introduced, respectively. Then, the role and/or effect of a wide diversity of nanostructured bimetallic electrocatalysts, including various alloying materials, electrocatalysts with distinct kind of interfaces, as well as some novel morphology will be covered with representative samples toward the improvement of catalytic activity, kinetics, charge/mass transport, selectivity, and stability. At the last, the challenges and perspective are presented to discuss the possible future work on nanostructured bimetallic electrocatalysts.

2. Fundamentals of water splitting

The overall efficiency of water splitting is undoubtedly a vital factor that determines the future of the large-scale applications. To this end, a good and in-depth understanding of reaction mechanism and rate/potential-determining steps is very necessary to gain insight into questions like how to rationally design and fabricate an ideal electrocatalysts and how to improve the design of an electrolyzer device for the reducing energy lost during energy conversion process. Therefore, in this section, we will briefly introduce some fundamental knowledge background regarding the well-accepted reaction mechanism and some necessary concepts for understanding the water splitting reaction. The related reaction pathways of HER and OER are presented firstly followed by the representative theoretically results obtained from density functional theory (DFT) calculations.

2.1. The overall reactions in water splitting

In an electrolyzer coupling with a stable power supply, water could be constantly split to hydrogen and oxygen (O_2) via two crucial multi-proton/electron coupled half-cell reactions, cathodic HER and anodic OER. According to the Nernst equation under standard conditions (25 °C, 1 atm), the thermodynamic voltage of this electrolyzer is estimated to be 1.23 V related to a reversible hydrogen electrode (RHE), regardless of the type of electrolyte[10]. Yet, due to the proton coupling nature, the specific reaction pathways occurring on cathode and anode, respectively, are dependent on the pH of the electrolyte, which are classified and listed in Eqs. (1) – (5).

Overall reaction:

$$H_2O \rightarrow H_2 + \frac{1}{2}O_2. \quad (1)$$

In acidic electrolyte:

$$2H^+ + 2e^- \rightarrow H_2\,(\text{Cathode}), \quad (2)$$

$$H_2O \rightarrow 2H^+ + \frac{1}{2}O^2 + 2e^-\,(\text{Anode}). \quad (3)$$

In neutral and alkaline electrolyte:

$$2H_2O + 2e^- \rightarrow H_2 + 2OH^-\,(\text{Cathode}), \quad (4)$$

$$2OH^- \rightarrow H_2O + \frac{1}{2}O_2 + 2e^-\,(\text{Anode}). \quad (5)$$

In practice, to initiate water splitting, high activation energy, sluggish kinetics, and poor energy efficiency need to be overcame, which demands a greater applied potential rather than 1.23 V decided by Nernst equation[3]. As such, the practical voltage of electrolysis can be expressed as Eq. (6),

$$V = 1.23 + \eta_a + |\eta_c| + iR, \quad (6)$$

where iR designates the ohmic potential drop owing to the resistance of ionic electrolyte, which cannot be avoided but can minimized by improving the electrolyzer setup. η_a and η_c represent the overpotential applied on the anode and the cathode, respectively, to activate the evolution of oxygen and hydrogen. This overpotential can be significantly influenced by various factors based on practical conditions, such as the resistance and activation energy of electrode materials, electrolyte diffusion rate, bubble evolution and desorption, as well as heat release. Therefore, many theoretical and experimental results have been proposed to understand the underlying reaction mechanisms, serving as a guide to rational design the electrocatalysts, cut-down the energy loss, accelerate the reaction rate, and finally promote the total cell efficiency.

2.2. Reaction pathways of HER

Regarding the pH of the electrolyte, the HER could take places based on either the Volmer-Heyrovsky or the Volmer-Tafel mechanisms. The specific reaction pathways are described below:

(1) Volmer steps: A reaction species adopts an electron at an active site to form an adsorbed hydrogen.

$$* + H^+ + e^- \rightarrow H^*\,(\text{In acid electrolyte}), \quad (7)$$

$$H_2O + e^- + * \rightarrow H^* + OH^-\,(\text{In alkaline electrolyte}). \quad (8)$$

(2) Heyrovsky steps: A reaction species (a proton or a molecular water) and an electron are adopted by adsorbed hydrogen to form a hydrogen molecule and then desorb from electrode surface.

$$H^* + H^+ + e^- \rightarrow H_2 + *\,(\text{In acid electrolyte}), \quad (9)$$

$$H^* + H_2O + e^- \rightarrow H_2 + OH^- + *\,(\text{In alkaline electrolyte}). \quad (10)$$

(3) Tafel step: Two adsorbed hydrogen atoms are coupled to produce a hydrogen molecule and the desorb from surface.

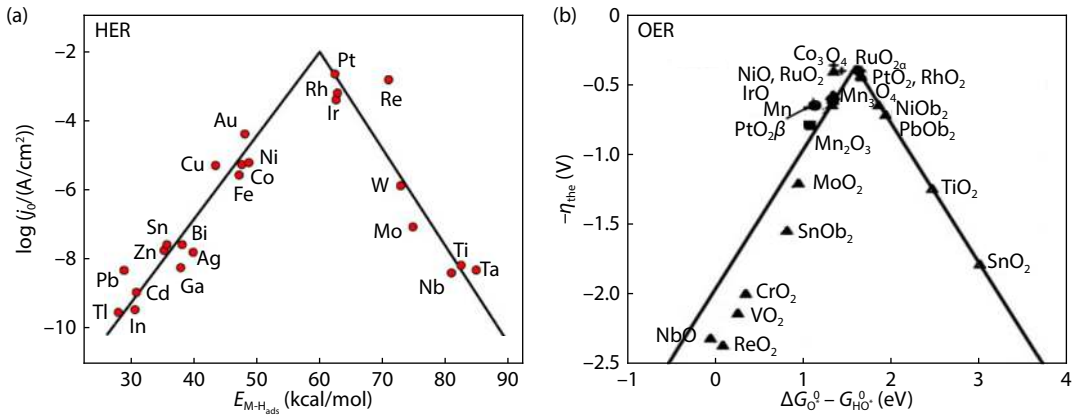

Fig. 1. (a) Volcano plot for the HER on metal electrodes in acidic media[20]. Reprinted with permission, Copyright 2010, American Chemical Society. (b) Activity trends for OER as a function of $\Delta G_{O^*} - \Delta G_{OH^*}$ for rutile and anatase oxides. The activity is expressed by the value of overpotential to achieve a certain value of current density[17]. Reprinted with permission, Copyright 2011, WILEY-VCH Verlag GmbH & Co. KGaA, Weinheim.

$$H^* + H^* \rightarrow H_2 + 2* \text{ (In acid or alkaline electrolyte)}, \quad (11)$$

where * represents an active site on electrode surface and H^* designates the adsorbed hydrogen atom. The initiation of HER always starts with Volmer steps (Eqs. (7) and (8)) to capture and fix a proton on electrode surface for the subsequently steps that may proceed through two pathways, either the electrochemical desorption via Heyrovsky steps (Eqs. (9) and (10)) or the chemical desorption via Tafel step (Eq. (11)).

From experimental results, the HER mechanism can be inferred by Tafel plot derived from the polarization curves[15]. In experiments, the linear scanning voltammetry (LSV) shows the response of current density to the applied potentials, which can be converted to Tafel plot as overpotential (η) vs. log(j) as described in Eq. (12), and the Tafel slope (b) is derived from the linear part of this plot[16]. The Tafel slope of ~30, ~40, and ~120 mV/dec correspond to Tafel, Heyrovsky, and Volmer steps respectively, which is readily used to disclose the rate-determining steps in practical HER. In addition, the Tafel slope is also a useful descriptor to evaluate the overall performance of both anode and cathode in practice. A smaller Tafel slope represents faster electrode kinetics and easier activation of catalytic reaction, which means electrodes can support a large current density even at a very low overpotential[17].

$$\eta = a + b\log(j). \quad (12)$$

Furthermore, as indicated in Volmer steps and Heyrovsky/Tafel steps, in HER, the chemical adsorption and desorption of H atoms are competing processes. According to the Sabatier principle, an excellent electrocatalyst should possess a suitable binding energy neither too strong nor too weak to not only facilitate the proton-electron-transfer process by adsorbing H^* tightly, but also accelerate the release of gaseous H_2 via facile bond breaking[18]. In other words, from a thermodynamics viewpoint, the constant evolution of hydrogen on the surface of the electrocatalysts could be considered as the process of reversible adsorption/desorption of H atoms on the active sites. Based on these assumptions, the Gibbs free energy change (ΔG_{H^*}) obtained from density functional theory (DFT) as described in Eq. (13), could be one of the key descriptors to theoretically predict the intrinsic activity for HER on different solid electrodes surface.

$$\Delta G_{H^*} = \Delta E_{H^*} + \Delta E_{ZPE} - T\Delta S, \quad (13)$$

where ΔE_{H^*} is the differential hydrogen chemisorption energy, ΔE_{ZPE} designates the difference of zero-point energy change between the adsorbed H* and gaseous H_2, ΔS is the entropy change, and T is the temperature[19–21]. In addition, considering the close correlation between the exchange current density (j_0) value and the thermodynamically derived Gibbs free energy, the establishment of the "volcano curve" (Figs. 1(a) and 1(b)) which is perfectly aligned with the Sabatier principle is another reference for rational design of ideal electrocatalysts[17–21].

2.3. Reaction pathways of OER

In terms of the OER, the proton coupling four-electron transfer involved process results in its sluggish kinetics and more possible reaction pathways compared with HER. Meanwhile, a well-accepted common sense indicates, in an alkaline electrolyte, a generated O_2 molecule inclines to form on a metal oxide/oxyhydroxide, rather than a metal surface or metal compound like phosphide, sulfide, etc[22, 23]. In other words, no matter which kind of electrode is used in practice, the electrocatalysts prefer to go through a pre-oxide process to form an in-situ grown oxide/oxyhydroxide thin layer with metal cations having higher oxidation states[24]. Thereby, the redox potential and electronic structure of metal cations after pre-oxide process is the key factors determining the activation energy of reactions and electro-kinetic profiles[25]. Same as HER, the reaction pathways of OER are also pH-dependent, and normally, the electron transfer process occurs in acid or alkaline as the sequence of equations shows below[26].

In acidic electrolyte:

$$* + H_2O \rightleftharpoons OH^* + H^+ + e^-, \quad (14)$$

$$OH^* \rightleftharpoons O^* + H^+ + e^-, \quad (15)$$

$$O^* + H_2O \rightleftharpoons OOH^* + H^+ + e^-, \quad (16)$$

$$OOH^* \rightleftharpoons +O_2 + H^+ + e^-. \quad (17)$$

In neutral and alkaline electrolyte:

$$* + OH^- \rightleftharpoons OH^* + e^-, \quad (18)$$

$$OH^* + OH^- \rightleftharpoons O^* + H_2O + e^-, \quad (19)$$

$$O^* + OH^- \rightleftharpoons OOH^* + e^-, \quad (20)$$

$$OOH^* + OH^- \rightleftharpoons * + O_2 + H_2O + e^-. \quad (21)$$

where * represents the active sites on the electrocatalysts surface, and OH^*, O^*, and OOH^* designate the intermediates adsorbed at the active sites, respectively. Apart from theoretical results mentioned before, some practical parameters are also worth highlighting here for comprehensive evaluation of the ability of a nanostructured electrocatalyst towards overall water splitting[27]. For instance, the concept of onset potential is basically identical to that of overpotential, except it designates the potential required to achieve a certain current density (the geometry normalized current density 10 mA/cm^2 is a well-accepted one), which is essential to reflect the net current density of electrodes. However, the geometry normalized current is inherently dependent on the catalyst loading or surface area, which neglects the contribution of enhancement of intrinsic activity per active site, and, thus, overlooks the superiority of interactions between distinct elements/components[28–30]. Given that, the electrochemically active surface area (ECSA) normalized current density is emerging as a more useful metric of intrinsic activity for electrocatalysts consisting of multi-elements or components demonstrated by recently studies related to highly active nanostructured electrocatalysts[31–33]. The ECSA normalized current density permits one to judge if higher activity of electrodes coming from a higher average turnover frequency or solely from an increased mass loading or number of active sites.

3. Recent progress of nanostructured bimetallic electrocatalysts towards water splitting

Over the last few decades, the noble metal-based (e.g. Pt, Ir, Ru, Pd, and Rh) electrode have been recognized as the most trusted and reliable catalysts for water splitting which can be readily explained by the "volcano plot". In terms of HER, the Pt locates at the summit of the HER activity volcano curve, so it can easily be understood why the Pt family materials were the commonly chosen electrode in an acid medium in early practice and research. As for OER, Ir/Ru based metal alloys and compounds due to advantageous electronic structure and suitable redox potential, have been proven as state-of-the-art electrocatalysts with low overpotential and Tafel slope. However, these noble metal family, even occupying the summit of the "volcano curve" naturally, always suffer from extreme scarcity of resource and/or severe corrosion, which disqualifies them as ideal electrodes in scalable applications that required extend working period. Meanwhile, the electrolyzer design for alkaline media offers opportunities for a wide range of bimetallic and/or metal-based multicomponent electrocatalysts serving as high-efficiency, low-cost, and long-term stable electrode. Since then, extensive studies have been devoted to developing strategies for design, fabrication, and improving the performance of nanostructure bimetallic-based electrocatalysts.

Up to now, most of the efforts have been aimed at either tuning the electronic structure, consequently, enhancing the intrinsic activity (higher average turnover frequency), or boosting the accessible active sites on the electrode surface. Commonly utilized strategies for metal-based catalysts, typically, can be classified into three main methods: 1) alloy involving multiple metallic elements with various composition ratios, which increase the intrinsic activity per active site of the electrocatalysts by tuning the electronic structure of the atoms on electrode surface[29, 34]. 2) Interface/substrate effects, which boost the intrinsic activity, particularly for electrocatalysts with poor electrical conductivity, by combining the advantages of electric properties of two distinct materials or the synergistic effect of the electronic coupling between the support and electrocatalysts[35, 36]. 3) Structure modifications in nano scale, which, on the one hand, enlarge the real surface area and expose more active sites to contribute to the net current density of electrode; on the other hand, some delicate structure adjustments could significantly affect the mass transport process and bubble evolution/desorption to achieve high performance[7, 24, 37, 38]. To a certain degree, the significant enhancement of electrocatalysts cannot solely be attributed to strategy, and, apparently, these strategies are always coupled and twined together for the improvement of overall cell efficiency. Therefore, in the following sections, we will begin our survey by briefly introducing some representative nanostructured bimetallic electrocatalysts that are classified based on the above summarized strategies and mechanisms.

3.1. Bimetallic alloying effect

The excellent intrinsic activity due to the inherent electronic structure of platinum group metals (PGMs), excludes the utilization of other non-precious transition metal as candidates for water splitting. However, the comparatively low activity of non-precious metal could be synergistically boosted via alloying materials[39, 40] which could cooperate with the interactions of different metal species with differing affinity toward various intermediates of interest. Specifically, transition metal alloy is predicted to tune the d-band electron filling, Fermi-level energy, and interatomic spacing[41], which could impact the electronic structure of the electrode surface and the binding energy of intermediates. Wang *et al.* reported solid-solution alloy nanoparticles of Ir and Cu first time in spite of being immiscible in the bulk, which prove the alloying effect at atomic-level inducing significant enhancement of activity[42]. Since Cu is a 3d metal whereas Ir is a 5d metal, the electron transfer from Cu to Ir is energetically favorable, consequently, the intimate interaction between Ir and Cu in the solid-solution alloy nanoparticles would affect the alloy properties and thus improve the performance. Additionally, with up to 56 at% of Ir substituted by Cu, the alloy electrode still possessed an excellent performance outperforming the monometallic Ir, which can be a promising candidate as a cost-effective catalysts. Besides Cu, other transition metal like Ni and Co can also alloy with Ir to serve as a promising candidate. Zhao *et al.* reported 3-dimentional nanoporous $Ir_{70}Ni_{30-x}Co_x$ microwires with excellent performance (220 mV @ j =

10 mA/cm^2), superior kinetics (Tafel slope = 44.1 mV/dec), and outstanding corrosion resistance (long-term stability) in acidic media[43]. Through the alloying effect, in the $Ir_{70}Ni_{30-x}Co_x$ alloy, the Ir atom on the surface possesses a higher valence state and low-coordination structure, which was proved as the real active sites to promote OER performance, and the reason for lower activation barrier relative to its mono-metal counterpart.

Although the noble metal involved alloying electrode could not only maintain superior activity and stability, but also significantly reduce the cost of electrocatalysts, the researchers still want to realize the noble metal-free electrode with competitive performance[44–47] by means of combination of other low-cost materials. Recently, research has demonstrated the utilization of carbon based material as well as transition metal alloys to achieve competitive activity and remarkable durability towards OER in alkaline[45]. Yang *et al.* demonstrated the ternary alloys encapsulated in graphene layers as an optimal bifunctional electrode to exhibit remarkable performance for HER and OER. The combination of single layer graphene and FeCoNi alloy directly tune the electronic structure on the surface resulting in the lower activation barriers, which lead to outstanding overall performance (1.7 V) comparable to that of the commercial Pt/RuO_2 couple, along with long cycling stability. Another study discovered, upon alloying effect, the crystal structure evolution of bimetallic alloy is also responsible for superior activity. The hcp crystal structure of NiFe alloy nanoparticles stimulate OER activity proposed by Wang *et al.*[47]. The experiments indicated, with different composition ratios and delicately tuning the thermal treatment process, the as-prepared hcp-NiFe possesses favorable electronic property to expedite reaction on surface, resulting in higher catalytic activity.

3.2. Interface effect

If the development of nanostructured bimetallic alloys is recognized as a promising strategy, the formation of interfaces between two distinct components would bring more possibilities for the performance-enhancement of electrocatalysts. Typically, the categories of interfaces in the field of electrocatalysts for water splitting include metal/metal interfaces[36], metal/compound interfaces[48–50], and metal or metal compound/conducting substrate interfaces[51–53]. The utilization of which type of interface highly depends on the synthesis method, materials used, and operating conditions in electrolyzer. For instance, in terms of many active transition-metal compound electrocatalysts, such as MoS_2[50], $CoSe_2$[54], NiFe layered double-hydroxide (LDH) and MnO_x[55], the inherently low electric conductivity suppresses charge transport and hence efficiency of electrocatalysis. To address this problem, the formation of interfaces between these active catalysts with metal, even with trace metal amounts, facilitates the charge transfer process and/or tuning local electronic structure for better activity. By chemical plating a thin layer of amorphous MoS_2 on the internal surface of nanoporous gold (NPG) to form a core-shell MoS_2@NPG (Fig. 2(a)), the electrode exhibited a 6-folder higher catalytic activity relative to the conventional MoS_2 in acidic media (Fig. 2(b)) and also excellent performance in neutral media due to the interplay induced by interface of gold and MoS_2 leading to fast electron transfer rate[50]. Moreover, the combination of gold nanoclusters with $CoSe_2$ demonstrated the electronic interactions between these materials can tune the bonding energy of one important intermediate (–OOH*)[54]. The Au25/$CoSe_2$ afforded a current density of 10 mA/cm^2 at small overpotential of ~ 0.43 V compared with the conventional counterpart ($CoSe_2$: ~0.52 V). Besides of favorably chemisorption of –OOH*, the tuned electronic structure of Au25/$CoSe_2$ also facilitated the desorption of O_2 molecules, which, as another origin, attributed to the enhancement of activity.

Apart from localized interfaces between nanoparticles, the interface formed on the current collector surface have also been investigated to explore the possible contribution to the performance of electrocatalysts. For instance, Desmond Ng and co-workers prepared thin film of $NiCeO_x$–Au onto Au-coated GC disk and bare GC disk, respectively to demonstrate the Au support effect[52]. The comprehensive comparison of activity between $NiCeO_x$–Au and $NiCeO_x$–GC (Fig. 2(d)) demonstrated the Au substrate is capable of improving the thin layer $NiCeO_x$ electrocatalyst. The DFT-U calculations (Figs. 2(e) and 2(f)) further confirmed the influence of Au substrate towards tuning chemisorption of intermediates and theoretical overpotential. Subsequently, Chakthranont and co-workers reported, compared to electrocatalysts loading on glass carbon (GC), the geometric current densities could be enhanced by loading electrocatalysts on Au substrate, e.g. NiCeOOH/Au (259 mV @ 10 mA/cm^2), and NiFeOOH/Au (140 mV @ 10 mA/cm^2) (Fig. 2(g))[53]. The experimental results from impedance spectroscopy and *in situ* X-ray absorption spectroscopy (Figs. 2(h) and 2(i)) attributed the enhancement of activity to the stronger physical adhesion of catalysts on Au, which leads to lower film resistances and higher number of electrochemically active metal sites. Lately, the substrate effect of transition metal is also discussed by Xiang *et al.*[49]. The FeNi LDH nanosheet arrays were directly grown on FeNi foil, and the obtained FeNi LDH/FeNi achieved ultrasmall overpotential (130 mV @ 10 mA/cm^2) and durable stability (over 10 h) in alkaline media (Figs. 2(k) and 2(l)). The DFT calculation revealed the hydroxide interfacial layer between LDH and FeNi substrate favored chemisorption of –OH* intermediate during OER and thereby reduced the overpotential required (Fig. 2(j)).

3.3. Nanostructured effect

Although tuning the electronic structure and thereby enhancing the intrinsic activity is a promising strategy towards improving the catalytic efficiency of electrocatalysts, the catalytic reaction only occurring on the electrocatalyst surface inspires the development of an electrode with nanostructured modification. To date, many template-assisted[56–58], electrochemical-deposited[59], thermal-treated[60–63], and surfactant-assisted syntheses[64–66] have been developed to fabricate electrocatalysts with numerous morphologies including nanoparticles with expected facet[67], nanowires with different diameters[43, 60], arrays structures[68–70], porous metal foam[71, 72], etc. The developed nanostructured electrocatalysts mainly aim to introduce more active sites per volume to supply higher exchange current density per geometric area compared with that of their bulk or film counterpart[73, 74] (Figs. 3(a) and 3(c)). For instance, Zhang and co-workers demonstrated porous monolayer nickel-iron layered double hydroxide nanosheets that could deliver a very low overpotential (230 mV @

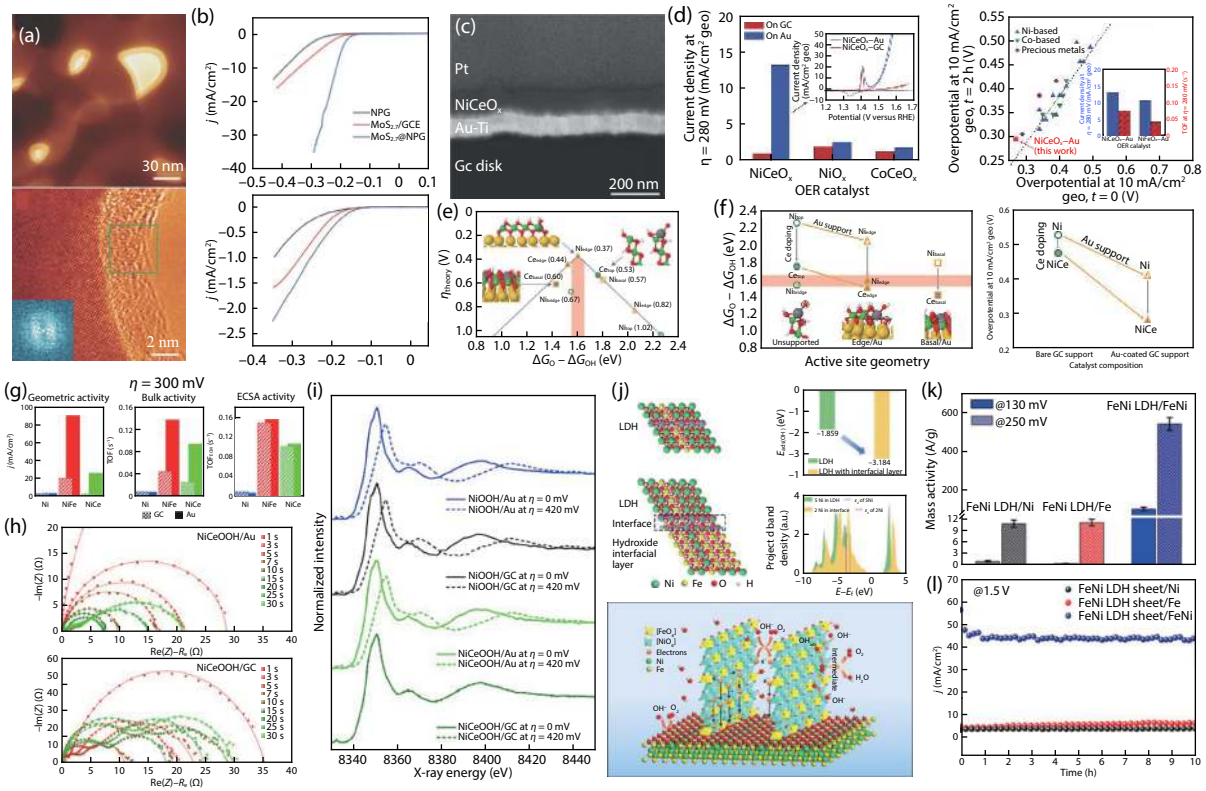

Fig. 2. (Color online) (a) Microstructure and interfaces of the molybdenum sulfide@NPG. (b) HER polarization curves of NPG, MoS_2@GCE, and MoS_2@NPG[50]. Reprinted with permission, Copyright 2014, WILEY-VCH Verlag GmbH & Co. KGaA, Weinheim. (c) Cross-sectional SEM image of the $NiCeO_x$–Au film. (d) Activity difference between $NiCeO_x$ supported on either Au-coated or bare GC disk, as well as OER performance of $NiCeO_x$–Au compared to those benchmarking catalysts reported. (e) Representation of the theoretical overpotential as a function of the difference in O^* and HO^* adsorption Gibbs energies. (f) DFT+U calculations illustrates the support effects on modifying performance of $NiCeO_x$–Au[52]. Reprinted with permission, Copyright 2016, Springer Nature. (g) Comparison of activity and (h) impedance spectra for Ni-based electrodes with various mass loading and composition. (i) In situ XAS of NiOOH and NiCeOOH on GC and Au substrates[53]. Reprinted with permission, Copyright 2017, American Chemical Society. (j) Adsorption sites and adsorption energies of OH on FeNi LDH and FeNi LDH with hydroxide interfacial layer, respectively. (k) Mass activity and (l) stability test of the FeNi LDH on foils at 1.5 V vs RHE for 10 h[49]. Reprinted with permission, Copyright 2018, American Chemical Society.

10 mA/cm^2) and Tafel slope (47 mV/dec)[72]. The unique porous monolayer structures with rich oxygen and cation vacancies was suggested as the main reason to enhance the adsorption of H_2O molecular and bond strength of *OH, and thereby significantly improved the OER performance. Gao *et al.* reported the highly nanostructured α-$Ni(OH)_2$ could attain a current density of 10 mA/cm^2 at a small overpotential of 0.331 V with a small Tafel slope of ~42 mV/dec, which obviously outperformed the β-$Ni(OH)_2$ nano-plate and nanoparticle, as well as the state-of-the-art RuO_2 electrocatalysts (Fig. 3(b))[74]. Moreover, the nanostructured α-$Ni(OH)_2$ also presented much better durability under cycling operating conditions compared to that of RuO_2. Indeed, apart from offering large effective surface area, another pivotal reason for designing the micro-/nano-structured electrocatalyst is its advantages regarding promoting the diffusions of ions and evolution of bubbles for outstanding durability. For example, Faber and co-workers proposed the morphology-dependent activity of cobalt pyrite (CoS_2) nanowire/microwire arrays (Fig. 3(d))[68]. In this work, CoS_2 nanowire/microwire array exhibited better HER performance (η = 145 mV @ 10 mA/cm^2) compared to the CoS_2 film. Meanwhile, microwire arrays exhibited remarkable stability (>40 h) due to promoted release of evolved H_2 gas bubbles from the electrode surface. Subsequently, Kim and co-workers proposed 3D ordered nanoporous nickel electrode that also possessed long-term stability, reporting a durability of smoothly working over 300 h (Fig. 3(e))[75]. The results demonstrated that the nanopores facilitate the release of tiny bubbles from the electrode surface, leading to fast refreshing of the electrolyte as well as superior durability of the electrode.

As an increasing number of research works have starting to concentrate on the role of nanostructuring on mass transport and electrode durability, recently, Song and coworkers revealed more detailed information about that by using assembled striped-pattern superlattices[37]. The template-assisted printing-based assembly of Pt nanocrystal nanoparticles (Fig. 4(b)) into striped-pattern (SP) superlattices (Fig. 4(a)) was fabricated with different width of gap. In comparison to drop-casting flat Pt nanoparticle films as well as Pt foil and Pt/C films, the SP superlattices exhibited improved efficiency (Fig. 4(c)) and durability (Figs. 4(d) and 4(e)) due to higher mass transference and smaller bubble stretch force. The SP_5 was found to possess the highest HER activity (14.3 mA/cm^2 @ η = 15 mV), which is significantly superior to the Pt/C (9.6 mA/cm^2 @ η = 15 mV), Pt films (4.5 mA/cm^2 @ η =

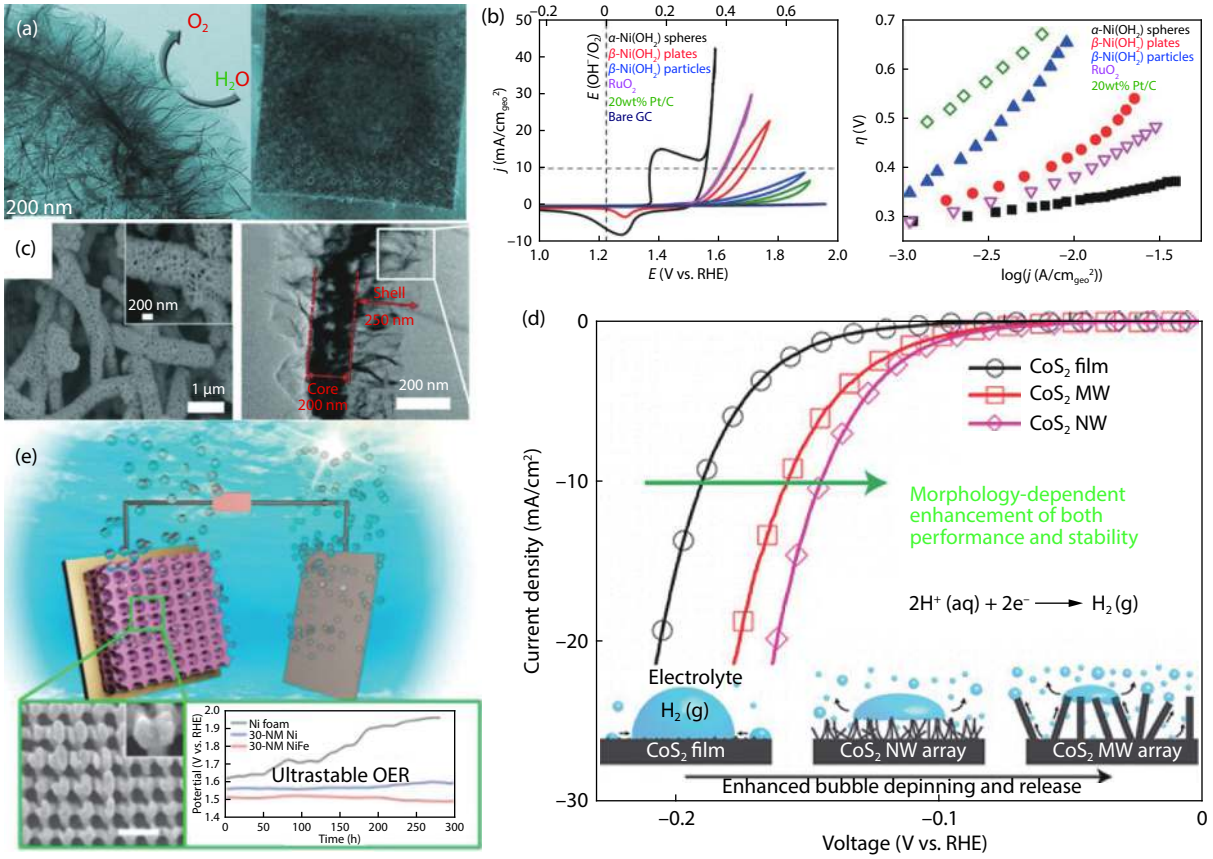

Fig. 3. (Color online) (a) SEM image of an α-$Ni(OH)_2$ hollow sphere and a digital photo of the nanosheet-assembled α-$Ni(OH)_2$ hollow spheres deposited on glassy carbon. (b) Comparison of CVs recorded at 100th cycle for bare GC electrode and modified GC electrodes comprising the α- and β-$Ni(OH)_2$ nanocrystals, RuO_2, and 20 wt% Pt/C and the corresponding Tafel slope[74]. Reprinted with permission, Copyright 2014, American Chemical Society. (c) SEM and TEM images for Cu@NiFe LDH for morphology characterization[60]. Reprinted with permission, Copyright 2017, Royal Society of Chemistry. (d) Polarization curves of CoS_2 film and CoS_2 nanowire/microwire array towards the morphology-dependent enhancement of both performance and stability. Bottom sketch describe the effect of morphology changing of CoS_2 towards the bubble evolution[68]. Reprinted with permission, Copyright 2014, American Chemical Society. (e) Illustration of 3D-nanomesh nickel electrode and the long-term stability tests of Ni foam, the 3D-nanomesh Ni electrode and the 3D-nanomesh NiFe electrode[75]. Reprinted with permission, Copyright 2018, Elsevier.

15 mV), and Pt foil (9.6 mA/cm^2 @ η = 50 mV). In this study, the SP superlattices were demonstrated to be capable of overcoming the two main issues relating the reactions involving gas evolution on a solid surface. One is the limited mass transfer rate due to adhered gas bubbles blocking the catalyst surface and resulting in a large number of inactive sites (Fig. 4(f)). Another one is the harmful stretch force (σ_f) from detachment of bubbles, which concentrated the local strain and destroyed the electrocatalysts, resulting in poor durability of electrode (Fig. 4(g)). The gas evolution process was monitoring and recorded (Figs. 4(h)–4(j)) to prove the advantages of nanostructuring effect. Apparently, the narrow gap width of SP_5 (5 μm) not only prevented the penetration of bubbles into spaces between the gaps, but also facilitated the small bubbles releasing from the electrode surface. As the width of gap increases to SP_{20} (20 μm), and then Pt films (Figs. 4(i) and 4(j)), more gas stick to the electrode surface, leading to a larger adhesive force between the bubble and the solid surface. Accordingly, the H_2 bubbles did not detach immediately, instead, the bubble adhered to the surface to grow large until the buoyant force is large enough to balance the adhesion force for bubbles taking-off. Furthermore, the gas evolution curves at 10 mA/cm^2 on different surface morphology could also explain the benefits induced by superlattice nanostructures. The stepped down current curve means the initiation of gas bubbles, once the bubbles detached, the current suddenly increased to the initial value. Therefore, the stable and straight i–t curves represented the fast bubbles releasing on the electrode surface.

4. Fundamentals of CO_2 reduction

Due solely to the final product (H_2 or O_2) resulting from water splitting, the reaction pathways and the number of intermediates are not that elusive and relatively easy to track down and confirm. Nevertheless, in electroreduction of CO_2, the reaction mechanism is far more intricate and are not fully understood. In 2012, the very first observation of a total of 16 different products from CO_2 reduction by Jaramillo's group unveiled the complex and intertwining nature of the CO_2 reduction pathways[76]. Normally, the CO_2 is stable in most scenarios, yet, under certain circumstances (usually demanding large energy cost and high-performance electrocatalysts), it could be reduced to a set of chemicals. Although extensive efforts have been made to reveal the possible intermediates, we are is still far from establishing a mature and comprehensive model to predict and tune the molecular behavior in the reduction process and hence improve the activity and selectivity for CO_2RR[77, 78]. Therefore, some well-accepted theoretical res-

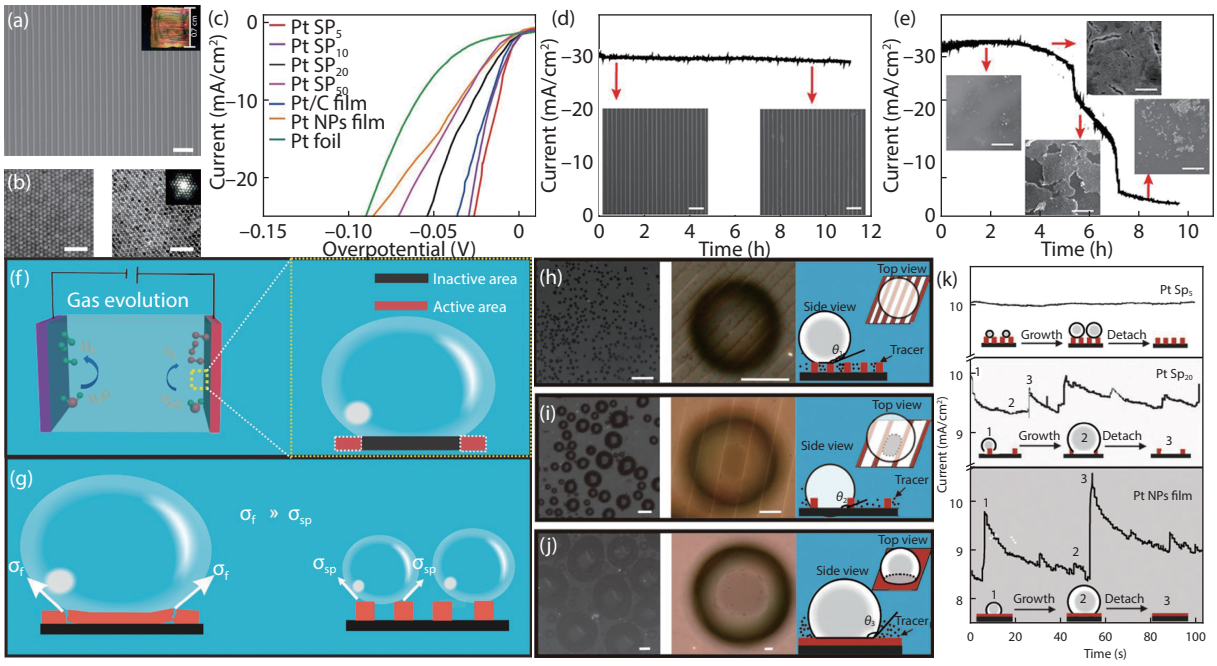

Fig. 4. (Color online) (a) SEM image of the large area SP superlattices and inserted photograph of the SP superlattices with dimensions 0.7 × 0.7 cm^2. (b) High-magnification SEM image of the long-rang-ordered Pt nanocrystals and TEM image of the nanocrystal superlattice. (c) Polarization curves of Pt SP_5, Pt SP_{10}, Pt SP_{20}, Pt SP_{50}, Pt NP film, Pt/C film and Pt foil electrocatalysts, the current density was normalized by geometry area. (d) Stability testing on Pt SP_5 for 11 h. (e) Stability testing on Pt NP films. (f) Schematic illustration of the growth of gas bubbles on a flat film electrode. (g) Schematic illustration of the stability difference between flat film and SP electrode. (h–j) Snapshots of digital videos taken during electrolysis at 10 mA/cm^2, magnified observations and schematic illustration of single bubble behavior on (h) Pt SP_5, (i) Pt SP_{20} and (j) Pt NP film. (k) *i*–*t* curves with a stable and straight curve in the case of Pt SP_5 and serrated curves on the Pt SP_{20} and Pt NP films[37]. Reprinted with permission, Copyright 2019, American Chemical Society.

ults regarding the key intermediates will be summarized firstly to help to understand the possible reaction pathways of nanostructured bimetallic electrocatalysts.

The reduction of CO_2 on the surface of heterogeneous catalysts involves the transformation of electrons and protons from/to the adsorbed CO_2 molecule. As an increasing number of electrons are transferred (from 2 electrons to 12 electrons), numerous possible reaction pathways and increasing intermediates are brought up. Yet, the initiating of CO_2RR always accompany the activation of CO_2 molecule that is widely recognized as a difficult step requiring large energy input due to the large kinetic barrier. Additionally, the equilibrium potentials of CO_2RR are located around 0 V (mostly in the range of –0.2 to 0.2 V vs. RHE), making the HER a competing reaction during activation of CO_2 to impair the selectivity of CO_2RR. The redox reactions related to the activation of CO_2 is considered as the following Eqs. (22)–(25)[5]:

$$* + CO_2 + H^+ + e^- \rightarrow {}^*COOH, \quad (22)$$

$$* + CO_2 + H^+ + e^- \rightarrow {}^*OCHO, \quad (23)$$

$$* + CO_2 + e^- \rightarrow {}^*CO_2^-, \quad (24)$$

$$* + H^+ + e^- \rightarrow {}^*H, \quad (25)$$

where * represents the active sites on the catalytic surface, while Eq. (25) is the competing hydrogen evolution reaction process. Eqs. (22) and (23) are well-accepted concerted proton-electron transfer reactions (CPET) involving a proton and an electron during the capture of the CO_2 molecule. As the 2e$^-$ transferred reduced products, the formation of either carbon monoxide (*CO) or formate (HCOO*) is dependent on the form of adsorbed active CO_2. Specifically, the bonding strength between the metal and the adsorbed species determines the selectivity in the first step. Metals, like Pb and In, that do not offer a strong M–C bond with CO_2 prefer to capture CO_2 via O atom and hence favor the formation of formate; while metals like Au and Ag, preferred to bind CO_2 via C, are more likely to generate CO. Consequently, *COOH and *OCHO are recognized as the key intermediates for producing CO and HCOOH, respectively[79]. The subsequent results have also demonstrated that formate/formic acid, normally, does not undergo further reduction under reductive conditions, serving as a terminal product in C1 group products[80]. Nevertheless, unlike formate, some experimental results related the reduction of CO on Cu confirmed CO as a crucial reaction intermediate for products with > 2e$^-$ transferred, as well as an important terminal product in C_1 group. The related theoretical studies help to explain the vital role of CO for further reduced products, such as methane, methanol, and oxygenates, regarding the bonding energy of adsorbed CO (*CO)[81–83]. Accordingly, when CO_2 is reduced to *CO in the first place, the bonding strength between metal and *CO determines the selectivity afterwards. Metals, such as Au and Ag, weakly bind to CO, leading to selective production of CO as terminal products. However, strongly bonding strength of *CO for metal results in inaccessible sites for CO_2RR and thus

leads to sites poisoning for favoring competing hydrogen evolution reaction. Given that, it is worthwhile highlighting the unique status of Cu here as a high-performance electrocatalysts due to its suitable intermediate binding energy between CO and Cu[83]. By far, most electrocatalysts that are capable of generating hydrocarbons and oxygenated without poisoning active sites still employed Cu-based materials for the electrodes. Furthermore, some Cu-based bimetallic electrocatalysts have also been indicated that are able to significantly suppress the competing HER due to site blocking effects and/or changes in *H binding energy[83–86].

Additionally, other form of intermediates, like formaldehyde (CH_2O), have been reported to produce methanol[87, 88] as well as trace amounts of methane[87, 89]. Subsequent experimental results reported the reduction of methanol and/or methane producing no products, suggesting methanol and methane are terminal products for C_1 group products[87]. Apart from conventional C_1 group products, the elaboration of reaction pathways from CO_2 or CO to C_{2+} products, typically ethylene and ethanol, have also been crucial subjects of experimental and theoretical studies for many years, due to their higher energy density and various applications. Besides dominant ethylene and ethanol, multi-carbon chemicals also include a wide range of aldehydes, ketones, and carboxylic acids[76]. In production of C_{2+} chemicals, the key factor is the C–C coupling process on catalytic surfaces. To date, two pathways have been demonstrated regarding the C–C coupling step: 1) *CO dimerizes to produce *OCCO species under low energy input[90]; 2) *CO is hydrogenated to produce *CHO species, the intermediate before formation of methane, requiring relatively large extra energy beyond equilibrium potentials[91]. As mentioned before, the copper-based electrodes are considered as traditional electrocatalysts capable of generating hydrocarbons and oxygenates in large amounts due to the suitable binding energy of *CO. Meanwhile, a few other electrocatalysts, such as PdAu, NiP, N-dopes carbon-based material, and NiGa, could also favors C–C coupling for multi-carbon compounds, but with comparatively low selectivity and efficiency with respect to Cu-based materials[92–95]. To date, the complete reaction pathway regarding C_{2+} products is still under development. Some experimental results partially reveal a possible mechanism. Ethylene has been demonstrated as the product of the reduction of ethylene oxide, suggesting the adsorbed epoxide as a possible intermediate for ethylene formation, whereas the ethylene glycol and oxalic acid are ruled out from possible reaction intermediates due to no products after reduction[87]. Additionally, glyoxal and glycoaldehyde are recognized as possible intermediates for the formation of acetaldehyde and ethanol[96, 97]. Furthermore, aldehydes were also reported by several experimental and theoretical results as a possible reaction intermediate in the formation of ethanol[98, 99].

Up to now, 5 possible terminal products in the C_1 group, including formate, CO, methanol, and methane, and other typical C_{2+} group products, such as acetaldehyde, acetic acid, ethylene, ethanol, and glycol, have been proven, and the comprehensive reaction pathways are also elaborated in Fig. 5[12]. Due to the complexity of the mechanism, we will not elaborate on it here exhaustively; more comprehensive discussions on the mechanism taking various tunable factors into account have been reported elsewhere[5, 11, 12].

5. Recent progress for nanostructured bimetallic electrocatalysts towards high-performance electrocatalysts for CO_2RR

As we discussed in a previous section, the reaction selectively produces formate or CO in the first step depending on how the electrocatalysts combine with CO_2 molecules. Only the formation of *COOH intermediate can be further reduced via combining with another proton and electron, yielding CO and H_2O. The generated CO paves the way for the formation of hydrocarbons and oxygenates from C_1 group products. According to the Gibbs free energy of adsorption towards various intermediates species obtained by DFT, a long-time thought classified the current active metal electrocatalysts for CO_2RR into 3 groups based on their selectivity[100–102]. However, even many types of pure metal electrocatalysts have been discovered and studied, most of them are still suffering from poor selectivity and large amount of by-products to produce high energy density multi-carbon products. In these cases, extensive studies have still concentrated on factors that affected the performance and selectivity, including the composition/component mixing for ideal electronic structure and/or suitable chemisorption energy toward specific species, catalyst surface structure/morphology modification. To this end, strategies including alloying with second metal, as well as bi-component electrocatalysts, have emerged and been proposed, suggesting the superior ability of altering the local electronic or combining the advantages of different materials for enhanced performance. Apart from that, it has been found that nanostructured catalysts with well-controlled structure, fine-tuning phase composition, and oxide-derived surfaces exhibited superiority for the selectivity and activity of CO_2 reduction. In this section, we will cover recent progress towards the development of nanostructured bimetallic electrocatalysts for the efficient conversion of CO_2. The electrocatalysts are mainly catalogized into bi-elemental alloy-based catalysts, bi-components based catalysts, and nanostructuring catalysts.

5.1. Bimetallic alloy effect

Early theoretical and experimental studies have widely employed pure metal[103–105] as the initial electrode for CO_2RR, however, the poor performance and stability of these curtailed their widespread applications[106–108]. Accordingly, alloying materials with the ability of mediation of various intermediates species via tuning electronic and/or geometric effects have attractive much interest. By far, the current common bimetallic electrocatalysts used for producing formic acid is predominantly a Pb-based[109, 110], Sn-based[111–113], and Pd-based[114–117] alloy. Extensive composition survey of various alloying determines the key factors that enhanced the performance. Kortlever *et al.* reported the Pd_xPt_{100-x}/C nanoparticles with very low onset potential for conversion of CO_2 to formic acid. Particularly, the $Pd_{70}Pt_{30}$/C exhibited a surprisingly high Faradaic efficiency of 88% toward formic acid after 1 h of electrolysis at – 0.4 V vs. RHE[114]. Subsequently, Jaramillo *et al.* synthesized thin films of AuPd via electron-beam co-deposition, suggesting Au and Pd can catalyzing synergistically to more active and selectively produce formate compare to the pure metals counterpart[115]. Later, the tin-lead alloys demonstrated its superb selectivity of 79.8% Faradaic efficiency on

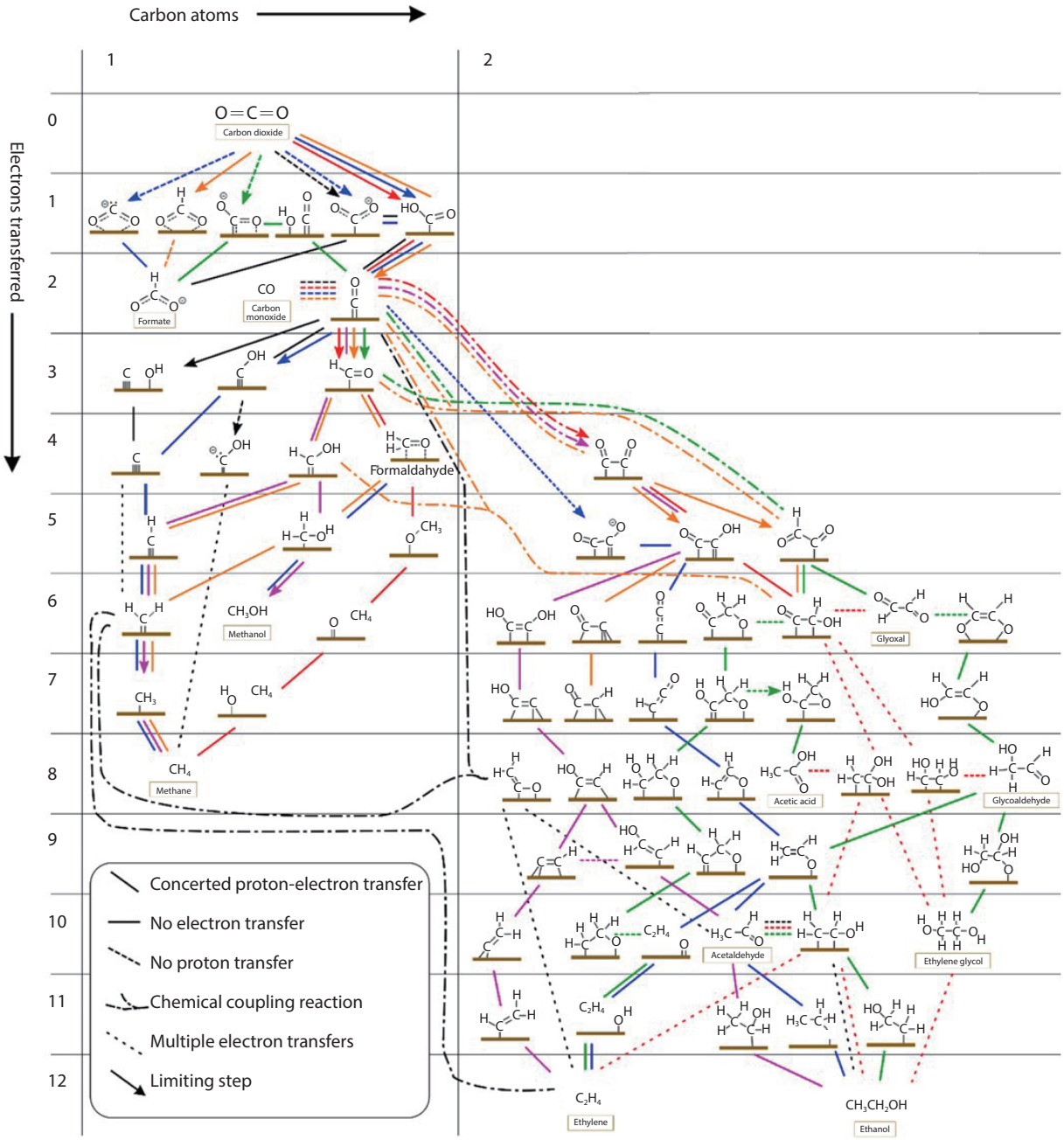

Fig. 5. (Color online) Possible mechanistic pathways of CO_2 reduction to C_1 and C_2 products[12]. Reprinted with permission, Copyright 2019, American Chemical Society.

the $Sn_{56.3}Pb_{43.7}$ electrode[109]. The results of XPS confirmed the excellent selectivity to the inhibition of forming low-conductive PbO film. By incorporating Sn in Pb, the Sn facilitated the formation of SnO_x as well as metallic lead (Pb^0), which significantly tuned the electrochemical behavior and hence the performance. Furthermore, PdSn alloy (Fig. 6(a)) was reported by Bai and coworkers for exclusive conversion of CO_2 into formic acid with nearly 100% Faradaic efficiency at –0.26 V overpotential[113]. In this study, systematically varying the PdSn composition was found to be able to produce the valley-shaped curve of Pd(0)/Pd(Ⅱ), which was recognized correlating with the activity and selectivity of CO_2RR. The DFT results further suggested that the optimal surface Pd–Sn–O configuration with highest oxygen occupancy facilitated the formation of HCOO* and suppressed the generation of CO and HER (Fig. 6(b)).

In terms of producing CO, Cu is frequently alloyed with other transition metalsin order to achieve high performance[118–127]. Among all the material candidates, CuAu alloys, as a promising electrode, have been widely investigated regarding composition-dependent activity[118], electronic/geometric effect toward high selectivity[120], theoretical prediction toward performance[119]. Kim *et al.* assembled uniform AuCu bimetallic nanoparticles with different compositions into ordered monolayers, suggesting the important synergistic geometric and electronic effect on enhanced activity. In this study, as the content of Au in this alloy increasing, the d band and the center-of-gravity position were gradually reduced in energy, which was confirmed by the high-resolution XPS (Fig. 6(c)). As a result, the degree of stabilization of intermediates can be varied by tuning the composition of Au–Cu (Fig. 6(d)). Similar composition-dependent electronic/geomet-

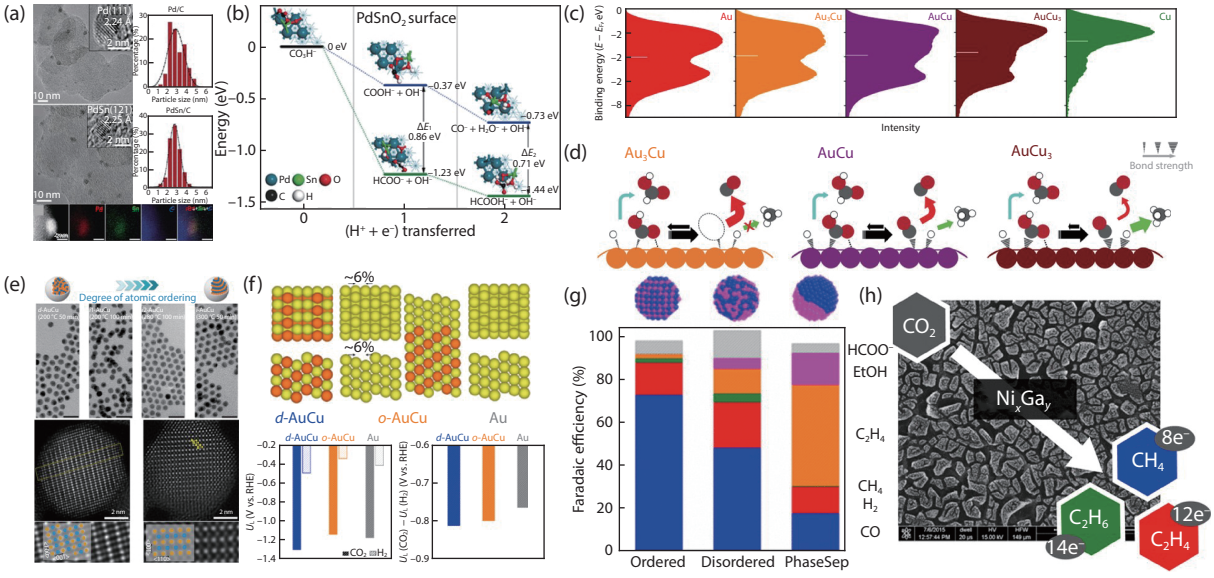

Fig. 6. (Color online) (a) Microstructural analysis and bulk compositions of the catalysts. (b) Calculated reaction energy profiles for CO_2 electroreduction to form CO (top) and HCOOH (bottom) on the $PdSnO_2$ surface[113]. Reprinted with permission, Copyright 2019, WILEY-VCH Verlag GmbH & Co. KGaA, Weinheim. (c) Surface valence band photoemission spectra of Au–Cu bimetallic nanoparticles. (d) Schematic showing the proposed mechanism for CO_2 reduction on the catalyst surface of Au–Cu bimetallic nanoparticles[120]. Reprinted with permission, Copyright 2014, Springer Nature. (e) The sketch of atomic ordering transformation of AuCu nanoparticles and the corresponding structural investigation. (f) Computational results of CO_2 reduction on AuCu surfaces. (g) The illustration of CuPd nanoalloys with different structures and the corresponding comparison of FE[125]. Reprinted with permission, Copyright 2017, American Chemical Society. (h) The SEM image of Ni_xGa_y alloying and the terminal products[95]. Reprinted with permission, Copyright 2016, American Chemical Society.

ric effect towards selectively producing CO are also demonstrated by the subsequent research in other alloy materials including PdCu[123, 124], CuCo[126], CuSn[122], and CuIn[121]. In addition to composition-dependent performance, Yang and coworkers further suggested that precise tune of elemental configurations within bimetallic nanoparticles could access the functional nanomaterials with significant enhancement of performance[125]. In this study, the effect of order-disorder transformation in AuCu nanoparticles on electrochemical CO_2 reduction were investigated in detail. The ordering transformation of a disordered AuCu (both 1 : 1 atomic ratio) under post-thermal treatment turned the inactive electrocatalysts, which went through HER, into an active electrocatalysts selectively producing CO with 80% Faradaic efficiency in the overpotential of ~200 mV. The transmission electron microscopy (TEM) along with thermochemical DFT calculations demonstrated the ordered lattice configurations in atomic level (Fig. 6(e)) and attributed this enhancement of selectivity and activity to the formation of compressively strained Au overlayers (Fig. 6(f)).

The direct conversion of CO_2 to hydrocarbons or multi-carbon oxygenates presents a striking route for the high energy density chemical fuels. Various Cu-based alloys, such as CuAu[128, 129], CuPt[130], and CuxZn[131], have been demonstrated as effective catalysts, which are capable of selectively producing hydrocarbons and multi-carbon oxygenate products such as methane, ethene, and ethanol. Nevertheless, the efficiency or selectivity of Cu-based alloy catalysts towards these products is largely limited by the competing HER and a wide range of byproducts due to large overpotential (typically > 0.7 V). Accordingly, Clark and co-workers reported compressively strained CuAg surface alloys with enhanced multi-carbon selectivity[132]. In this paper, the appearance of small amount of Ag into Cu surface induced compressive strain in the neighboring Cu atoms and, consequently, resulted in a shift in the valence band density of states of Cu. As a result, the Cu(100)-Ag surface alloy enabled the suppression of HER as well as selective generation of multi-carbon oxygenates like ethane with 35% Faradaic efficiency, which is more than double the total oxygenate Faradaic efficiency observed for pure metal. Subsequently, the influence of ordered, disordered, and phase-separated CuPd alloy on product selectivity was proposed by Kenis and co-workers[133]. A wide range of bimetallic CuPd with ordered, disordered, and phase-separated atomic arrangements were studied to unveil the key factors toward high selectivity for C_1 or C_{2+} (Fig. 6(g)). The ordered CuPd nanoparticles showed highly selectivity (FE > 80%) toward the formation of C_1 group products, while the phase-separated CuPd selectively produced C_{2+} group products (FE > 60%). The authors indicated that the Cu atoms in phase-separated one favored the *CO to be dimerized to OC-COH that, subsequently, was mainly converted into C_{2+} group products with a small amount of conversion to CH_4. Meanwhile, in the ordered CuPd nanoparticles, the *CO preferred to form CHO intermediate adsorbed on Pd atom via oxygen atoms, which stabilized the CHO strongly for further production of CH_4. Accordingly, the dimerization of adsorbed CO displayed a vital role upon the following reaction pathways. Apart from Cu-based alloying elements, Torelli and co-workers proposed conversion of CO_2 to highly reduced C_{2+} products, ethylene and ethane, as well as the fully reduced C_1 products, methane, on three different phases of non-precious transitional metal-based NiGa films (Fig. 6(h))[95]. In this paper, the onset potential for producing CH_4, ethylene, and ethane was proved to be –0.48 V vs. RHE, which was the lowest overpotential reported to date for the production of

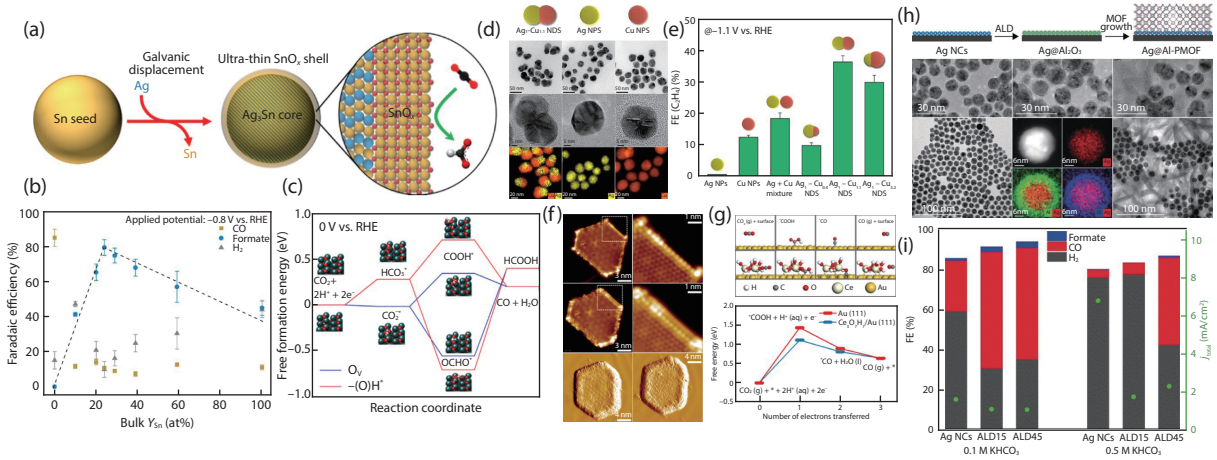

Fig. 7. (Color online) (a) A schematic illustration of the Ag_3Sn core-shell structure. (b) CO_2 reduction Faradaic efficiencies of AgSn/SnO_x. (c) The most favorable free energy pathways of CO and HCOOH formation on SnO with Ov and –(O)H*, respectively[112]. Reprinted with permission, Copyright 2017, American Chemical Society. (d) Schematic and TEM characterization of the three types of Ag/Cu nanocrystals. (e) The schematic illustration and activity comparison of Ag NPs, Cu NPs, and AgCu alloy with various composition ratio[137]. Reprinted with permission, Copyright 2019, American Chemical Society. (f) Interaction between CeO_x/Au(111) and CO_2 (g) DFT calculations of CO_2RR at 0 V vs RHE on Au(111) and $Ce_3O_7H_7$/Au(111) surfaces[134]. Reprinted with permission, Copyright 2017, American Chemical Society. (h) Schematic illustration of the synthesis process and the corresponding morphology and composition characterization of the Ag@Al-PMOF. (i) FEs and total current densities for Ag NCs and Ag@Al-PMOF hybrids with different MOF thicknesses[138]. Reprinted with permission, Copyright 2017, WILEY-VCH Verlag GmbH & Co. KGaA, Weinheim.

multi-carbon oxygenates and CH_4.

5.2. Bi-component effect

In addition to utilizing alloying electrocatalysts with varying composition and mixing patterns to directly adjust surface electronic/structure environments, bi-component catalysts, that are able to combine distinct catalytic/electronic properties of each single-component counterpart, have emerged as another pronounced electrocatalyst. Some experiments demonstrated that the enhanced performance towards different hydrocarbons and oxygenates was due to the generated various interfaces. Luc and co-workers reported Ag–Sn bimetallic core-shell structure for selective conversion of CO_2 to formic acid (Fig. 7(a))[112]. In this work, the optimal SnO_x shell thickness of ~1.7 nm exhibited a high formate Faradaic efficiency of ~80% (Fig. 7(b)) and a formate partial current density of ~16 mA/cm^2 at –0.8 V vs. RHE, suggesting a remarkable performance compared to the state-of-the-art electrocatalysts. The DFT calculations suggested that the oxygen vacancies on the SnO(101) surface were responsible for the enhanced performance by tuning the adsorption towards OCHO* and COOH* (Fig. 7(c)). Subsequent research related to the bimetallic interfaces, such as Au-island on Cu[112], Au–CeO_x interface[134], Au embedded in graphene nanoribbons[135], Ag–Cu biphasic boundaries[136], and Ag–Cu nanodimers[137], were also investigated toward selectively formation of CO, methane, and multi-carbon oxygenates. For instance, the Au–CeO_x exhibited much higher activity and Faradaic efficiency than single CeO_x or Au that was recognized as the most active pure metal electrocatalyst for CO formation. The enhanced activity was attributed to the promoting adsorption and activation of CO_2 on Au–CeO_x interface observed by in situ scanning tunneling microscopy and synchrotron-radiation photoemission spectroscopy (Fig. 7(f)). The DFT calculation indicated the synergy between Au and CeO_x enabled the stabilization of carboxyl intermediate and thus facilitated the selective formation of CO (Fig. 7(g)). Furthermore, Huang and co-workers synthesized the Ag–Cu nanodimers with tunable interface to investigate the benefit of multicomponent catalysts toward CO_2RR (Fig. 7(d))[137]. The Ag–Cu nanodimers with different Cu domain sizes (Ag_1–$Cu_{0.4}$, Ag_1–$Cu_{1.1}$ and Ag_1–$Cu_{3.2}$) were carefully synthesized by different precursor and reducing agents. The resulting Ag–Cu nanodimers exhibited different selectivity, among which, Ag_1–$Cu_{1.1}$ nanodimer showed a 3.4-fold Faradaic efficiency improvement toward C_2H_4, as well as 2-fold enhancement in the overall activity compared to the Cu nanoparticles with similar size and morphology (Fig. 7e).

Besides bi-component electrocatalysts consisting of metal/metal interfaces, other form of combination are also promising for CO_2RR. For instance, Guntern and co-workers reported novel nanocrystal/metal-organic framework hybrids, Ag@Al-PMOF, as the electrocatalysts (Fig. 7(h)) to realize the CO_2 conversion with relatively high Faradaic efficiency[138]. The experimental results demonstrated that, over the entire potential range (–0.9 to –1.4 V vs. RHE), the Ag@Al-PMOF displayed a decreased FE for H_2 and increased FE for CO and formate compared to the bare Ag nanocrystals (Fig. 7(i)). The highest FE of CO was 55.8% at –1.1 V vs. RHE, which is almost 2.2 times higher than the Ag nanocrystals. Meanwhile, the combination of Cu nanoparticles with N-doped graphene oxide was also demonstrated as a high-performance electrocatalyst for CO_2 conversion by Yuan and co-workers. In this work, CO_2 could be efficiently converted into ethanol at an overpotential as low as 0.14 V while achieving maximum FE for ethanol of 56.3% at –0.25 V vs. RHE[139]. Meanwhile, these Cu decorated graphene oxide sheets could retain stable activity after 24 h of continuous working, suggesting the pronounced durability of this electrode. These exciting activity, selectivity and durability could be attributed to the large surface area provided by graphene oxide, enhanced CO_2 adsorption as well as very low electron transfer resist-

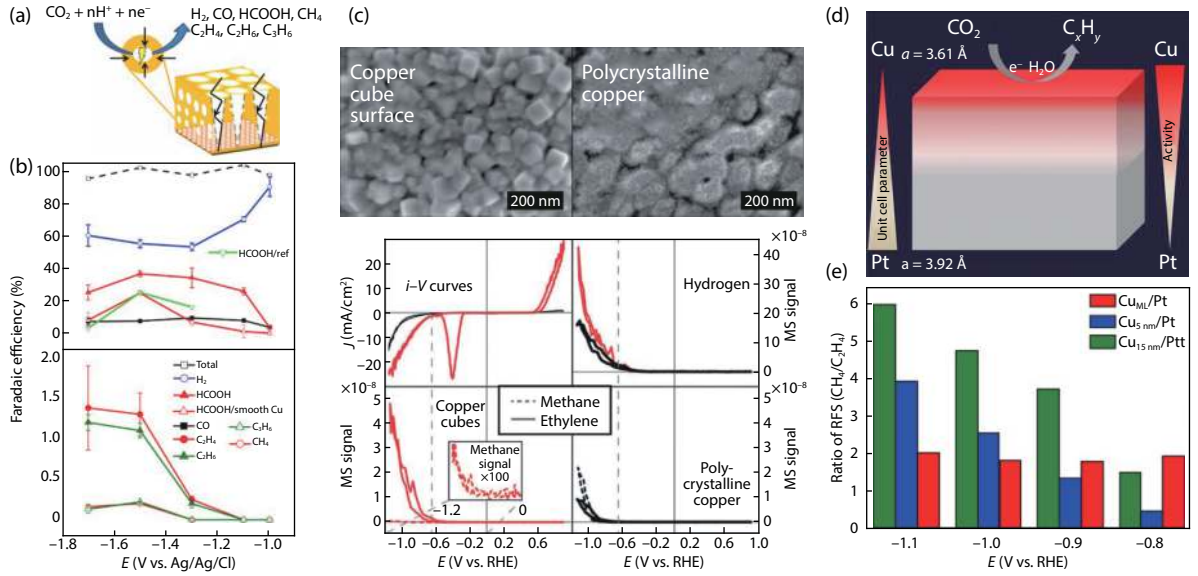

Fig. 8. (Color online) (a) Schematic illustration of the structure of Cu nanofoams and the terminal products. (b) Product distribution as a function of applied potential during the electrochemical reduction of CO_2[145]. Reprinted with permission, Copyright 2014, American Chemical Society. (c) SEM images of the Cu cube surface and cyclic voltammograms of Cu cube and polycrystalline cupper surface towards formation of H_2, methane and ethylene[146]. Reprinted with permission, Copyright 2015, WILEY-VCH Verlag GmbH & Co. KGaA, Weinheim. (d) Schematic showing the Cu overlayer structure-dependency over the formation of hydrocarbons. (e) Ratios of RFSs for CH_4/C_2H_4 on different thicknesses of the Cu layer deposited on a pure Pt substrate obtained from the CO_2 reduction experiments[147]. Reprinted with permission, Copyright 2013, American Chemical Society.

ance in this system.

Copper involved bi-component tandem electrocatalysts that could conduct two and/or more sequential steps of CO_2RR is also a promising strategy to realize targeted C_{2+} products. For instance, Carlos and co-workers reported the discovery of gold nanoparticles deposited on a polycrystalline copper foil (Au/Cu) as a novel electrocatalyst that is highly active towards formation of alcohols[140]. In this work, the gold nanoparticles were demonstrated to accumulate the generated CO on the nearby copper to facilitate the C–C coupling and thereby improve the activity for further reduced alcohols like ethanol and n-propanol. As a consequence, the Au/Cu electrocatalysts are over 100 times more selective for the C_{2+} group products containing the C–C bonds over the C_1 products like methane or methanol, which is significantly superior to pure gold, copper or AuCu alloys. The similar facilitation of C–C bond formation for producing C_{2+} group products with high selectivity was also demonstrated on the Ag-core-porous-Cu-shell nanoparticles by Peter and co-workers[141]. By mimicking the multistep cascade reactions in enzymes, the as-prepared Ag core surrounded by a porous Cu shell could not only confine CO_2 and the generated CO inside this architecture, but also separate active sites spatially to facilitate the C–C coupling process. Specifically, Ag core reduced CO_2 to CO firstly which would migrate and gather into the porous shell due to the nanoconfinement effect. The high-concentration CO_2 and CO adsorbed on the porous Cu was suggested to highly favor the C–C coupling process in CO_2RR. As a result, this unique architecture of Ag core and porous Cu shell was able to yield n-propanol and propionaldehyde at –0.6V vs. RHE potentials. Later, some mechanistic and theoretical results stated the reaction pathways of enhanced hydrocarbons for Cu involved tandem electrocatalysts[142, 143]. By using operando DEMS and time-resolved isotope-labelling experiments, Wang and co-workers reported the beneficial effect of using mixed CO/CO_2 gas-fed on CuO_x nanoparticles towards the C_2H_4 yields, which indicated that the enhanced generation of C_2H_4 was mainly attributed to the *CO (from CO)-*CO (from CO_2) cross-coupling pathway[142]. Meanwhile, they also demonstrated that the co-fed CO didn't compete with CO_2 for adsorption sites, suggesting separate and non-scrambling reactant adsorption sites for CO_2 and CO respectively during CO_2RR. Given that, they proposed the concept of internal co-feeds on tandem electrocatalysts to explain the enhancement of ethylene on bimetallic CuO_x–NiNC tandem catalysts. To be specific, the high-surface-area Ni-N-functionalized carbon served as the CO producer to reduce and accumulate extra *CO during CO_2RR which was subsequentially consumed and reduced to ethylene on the CuO_x particles via cross-coupling process.

5.3. Nanostructured effect

Under certain conditions, the distinct activity and improved selectivity regarding bimetallic electrocatalysts might be attributed to the nanostructuring effect[144–149] via fine regulation of morphology and electronic structure. Typically, by forming defects on the surface, controlling particle size and interparticle distance, as well as tuning the exposed crystal faces and coordination number of the active sites, the local electronic structure of electrocatalysts can be changed accordingly, and thus tuning binding energy of intermediates of interest for improved activity and selectivity. Given that, Sen and co-workers reported that, with respect to the smooth copper surface, the pure copper foams with hierarchical porosity directly affected the distribution of terminal products and the corresponding Faradaic efficiency (Fig. 8(a))[145]. In this work, experimental evidence suggested the reaction pathways of CO_2RR was altered by the nanofoam morphology, leading to

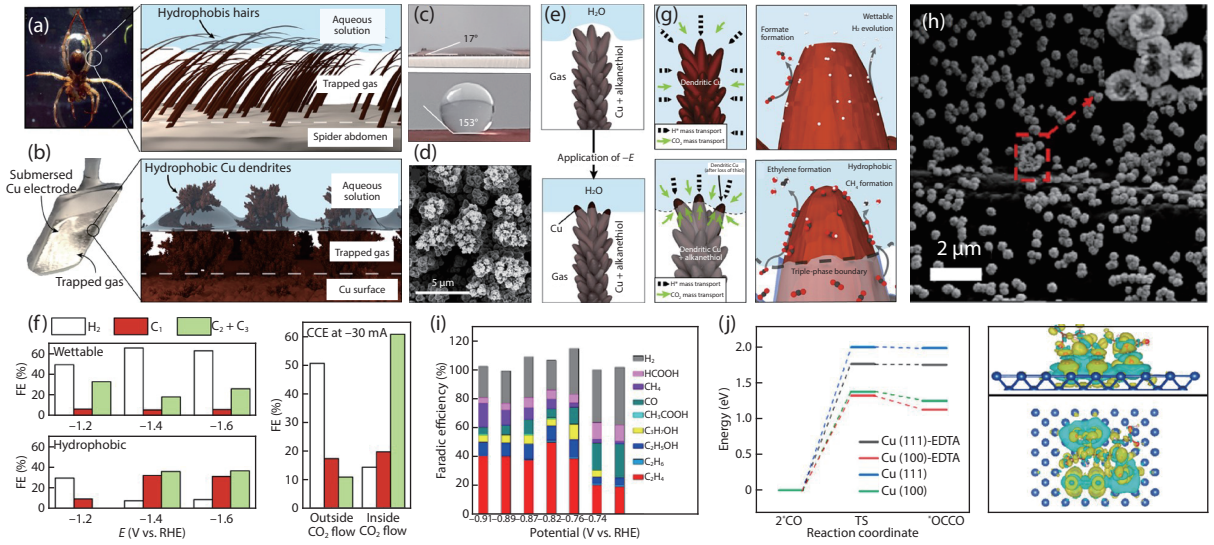

Fig. 9. (Color online) (a) This is illustrated on a diving bell spider for subaquatic breathing. (b) A hydrophobic dendritic Cu surface for aqueous CO_2 reduction. (c) The contact angle measurements of the wettable and hydrophobic dendrite. (d) SEM image of the hydrophobic dendrite. (e) Illustration of the hydrophobic dendrite gaining a solid–liquid interface on the application of a negative potential. (f) CPE product FEs from the wettable and hydrophobic dendrite at various potentials. (g) The proposed role of hydrophobicity in promoting CO_2 reduction over proton reduction[140]. Reprinted with permission, Copyright 2019, Springer Nature. (h) SEM images of EDTA modified porous hollow cupper sphere. (i) FE of all the reduction products for H-Cu MPs at various potentials. (j) Free energy profiles for the CO dimerization reaction on surfaces with or without EDTA modification[149]. Reprinted with permission, Copyright 2020, American Chemical Society.

the boosting FE of formate at all potentials and, particularly, 26% top at –1.1 V vs. RHE with respect to 3% at smooth surface. Meanwhile, the FE of CO, methane, and ethylene notably decreased; whereas the ethane and propylene appeared to be detectable (Fig. 8(b)). Subsequently, the results about copper nanocube with high selectivity towards ethylene was reported, suggesting the significant influence of nanostructured surface upon the activity and selectivity of CO_2RR[146]. In this work, the experimental evidence from online electrochemical mass spectrometry (OLEMS) demonstrated the ethylene selectivity of Cu nanocubes (Fig. 8(c)), suggesting this cubic nanostructure strongly favored the formation of multi-carbon products after comparison with the products of various different copper surface. Besides, extensive studies on the Cu overlayer films were also reported. Reske *et al.* reported the influence of combining the Pt substrate with Cu overlayer films toward the performance of CO_2RR[147]. With decreasing thickness of Cu layer, larger drop of amount for methane with respect to ethylene indicated that the selectivity for methane or ethylene significantly exhibited high thickness-dependence (Fig. 8(d)). With thicker layer (15 nm), the Cu overlayer film behaved more like bulk Cu, resulting in methane products 6 times higher than ethylene at –1.1 V vs. RHE; whereas the production ratio of methane over ethylene dropped to 2 : 1 at –1.1 V vs. RHE with thinner Cu overlayer.

Apart from directly mediating the morphology of catalysts for higher activity and selectivity, another merit of nanostructured electrocatalysts is its ability to affect the hydrophobicity of the electrode as well as the local pH around the catalyst surface, which results in the inhibition of competitive reaction (HER) and the promotion of CO_2RR. For instances, Nam and co-workers reported a superhydrophobic surface of hierarchically structured Cu dendrites that could surprisingly achieve 56% FE for ethylene and 17% for ethanol production, comparing to poor FE of 9% and 4% on a hydrophilic and wettable equivalent[148]. Accordingly, this idea was inspired by the diving bell spider (Fig. 9(a)) of which the hydrophobic hairs on their plastrons could trap air and allow them to breath underwater. The similar multiscale hydrophobic surface could be also achieved by hierarchically structured dendritic Cu treated with 1-octadecanethiol to form a monolayer of alkanethiol (Fig. 9(d)), and the visibly trapped bubbles (Fig. 9(b)) along with the difference of contact angle before and after 1-octadecanethiol treatment (Fig. 9(c)) demonstrated its superior hydrophobicity. After initially applying potential on this electrode, a stable liquid-electrode-gas triple-phase boundary was formed (Fig. 9(e)) for the proceeding CO_2RR. Comparing with the wettable electrode, the hydrophobic dendrite Cu significantly decreased the evolution of H_2 and increased the FE of C_1 and C_2 products in wide range of potential, and especially at –1.6 V vs. RHE, the hydrophobic dendrite impaired the FE of H_2 production below 10%, whereas the efficiency for both C_1 and C_2 products exceeded 30% and ~35%, respectively (Fig. 9(f)). The author explained this trend by indicating that, compared to hydrophilic electrode surface, the CO_2 could accumulate in the electrolyte-solid-gas triple-phase boundary at the electrode surface while pushing the electrolyte and thereby the H^+ away from the surface. In that case, the surface concentration of Cu-COOH* and the subsequently formed Cu–CO* is dramatically increased over that of Cu–H*. Consequently, the C–C coupling process was promoted, while the H_2 evolution was significantly suppressed (Fig. 9(g)). Later, Liu and coworkers reported the EDTA anions-modified porous hollow copper microspheres (Fig. 9(h)) could double the FE of ethylene from 23.3% to 50.1%, which is the highest efficiency towards ethylene among all kinds of Cu-based electrodeposited catalysts[149]. In this work, the products of this EDTA modified porous hollow copper included ethylene, ethanol, n-propyl alco-

hol, formic acid, methane, and carbon monoxide, exhibiting 67.3% FE of multi-carbon products and 86% FE of overall CO_2RR (Fig. 9(i)). The DFT calculations indicated that this surprising enhancement of FE could be attributed to the EDTA-modified local-charged copper surface, which could synergistically stabilize transition state and dimer (Fig. 9(j)).

6. Summary and perspectives

The development of highly efficient and durable electrocatalysts is essential for the wide-spread application of various energy conversion systems. To date, bimetallic electrocatalysts with morphology modification in the nano scale have been recognized as a promising options. In this review, fundamental knowledge background and vital concepts in theoretical studies for water splitting and CO_2RR are covered firstly to understand the exact process happening on the surface of nanostructured bimetallic electrocatalysts. After that, the dominant advantages of these electrocatalysts was summarized to bimetallic alloying, bi-component interfacing, and nanostructuring, which could result in electronic environment alterations of surface atoms, coupled benefits of two distinct materials regarding different electronic properties, and fine-design structure modifications in the nano scale for fast mass/proton/electron transformation. Despite these significant progresses, there are still many challenges and questions, which must be addressed before the nanostructured bimetallic catalysts can find a wide range of practical uses.

(1) In the current stage of nanostructured bimetallic electrocatalysts developed for water splitting, the in-situ spectroscopic study is extremely lacking. Although the development of DFT calculation already provides a useful theoretical tool to identify and predict the active sites and electronic structure change, the further design and optimization of performance of electrocatalysts is highly reliant on the exact catalytic mechanism on these structure/electronic tuned catalysts where a straightforward observation of catalytic reaction process under various in-situ spectroscopic techniques could be very promising for that goals. Especially for these nanostructured bimetallic electrocatalysts, the fine-tuning structure in nano scale significantly alter the bubbles evolution process for fast kinetics and mass transferring, but, lots of unknown questions, like have these structure modification affected strain or resistance in bulk, is left behind, which need to be unraveled by directly investigation of the structure/bubbles evolution behavior. On the other hand, the precise identification of catalytic sites is essential for unveiling how the interaction between two metals or interfaces between two components boosts the activity of reactions, which can be experimentally verified through in-situ observation in atomic-level.

(2) As for CO_2RR, advanced in situ characterization techniques are also necessary for an in-depth understanding of the reaction pathways and to improve the activity and/or selectivity for further rational design of nanostructured bimetallic electrocatalysts. In fact, the in situ FT-IR is already used for unravelling the reaction pathways and intermediates by providing the information about adsorbed carbon species on catalysts[150–152]. However, there is the same dilemma as water splitting; experimental results barely provide directly observation using in situ spectroscopic techniques in a proceeding CO_2RR to identify the real active sites or explain the enhancement of performance, not to mention the observation of relationship between the performance enhancement and the rational-design sophisticated nanostructure. In addition, considering the complexity of the local chemical environment near or on the catalyst surface, such as surface intermediate coverage, local pH, regulation of reactant and product diffusion at interfaces, and local electric field, a quantitative understanding of the correlation between the local reaction conditions and the CO_2RR product selectivity is important but fundamentally challenging. This is largely due to the intertwined nature of numerous parameters and the ill-defined structure of the most investigated electrodes. Therefore, a simple tandem electrocatalyst model with well-defined and programmable architecture, composition, and the interface will be highly desirable to give a quantitative prediction of the relationship between the structure/materials and the selectivity of the electrode, as well as to guide the fabrication of practical CO_2RR electrodes in the future.

References

[1] Fu G, Lee J M. Ternary metal sulfides for electrocatalytic energy conversion. J Mater Chem A, 2019, 7, 9386

[2] Tahir M, Pan L, Idrees F, et al. Electrocatalytic oxygen evolution reaction for energy conversion and storage: A comprehensive review. Nano Energy, 2017, 37, 136

[3] Li X, Hao X, Abudula A, et al. Nanostructured catalysts for electrochemical water splitting: Current state and prospects. J Mater Chem A, 2016, 4, 11973

[4] Gao D, Arán-Ais R M, Jeon H S, et al. Rational catalyst and electrolyte design for CO_2 electroreduction towards multicarbon products. Nat Catal, 2019, 2, 198

[5] Birdja Y Y, Pérez-Gallent E, Figueiredo M C, et al. Advances and challenges in understanding the electrocatalytic conversion of carbon dioxide to fuels. Nat Energy, 2019, 4, 732

[6] Shao Q, Wang P, Huang X. Opportunities and challenges of interface engineering in bimetallic nanostructure for enhanced electrocatalysis. Adv Funct Mater, 2019, 29, 1806419

[7] Niether C, Faure S, Bordet A, et al. Improved water electrolysis using magnetic heating of FeC-Ni core-shell nanoparticles. Nat Energy, 2018, 3, 476

[8] Wang Y, Yan D, El Hankari S, et al. Recent progress on layered double hydroxides and their derivatives for electrocatalytic water splitting. Adv Sci, 2018, 5, 1800064

[9] Gong M, Dai H. A mini review of NiFe-based materials as highly active oxygen evolution reaction electrocatalysts. Nano Res, 2014, 8, 23

[10] Yan Y, Xia B Y, Zhao B, et al. A review on noble-metal-free bifunctional heterogeneous catalysts for overall electrochemical water splitting. J Mater Chem A, 2016, 4, 17587

[11] Zhang L, Zhao Z J, Gong J. Nanostructured materials for heterogeneous electrocatalytic CO_2 reduction and their related reaction mechanisms. Angew Chem Int Ed, 2017, 56, 11326

[12] Nitopi S, Bertheussen E, Scott S B, et al. Progress and perspectives of electrochemical CO_2 reduction on copper in aqueous electrolyte. Chem Rev, 2019, 119, 7610

[13] Gao M Y, Yang C, Zhang Q B, et al. Facile electrochemical preparation of self-supported porous Ni-Mo alloy microsphere films as efficient bifunctional electrocatalysts for water splitting. J Mater Chem A, 2017, 5, 5797

[14] Cheng C, Zheng F, Zhang C, et al. High-efficiency bifunctional electrocatalyst based on 3D freestanding Cu foam in situ armored CoNi alloy nanosheet arrays for overall water splitting. J Power Sources, 2019, 427, 184

[15] Ghosh S, Basu R N. Multifunctional nanostructured electrocata-

lysts for energy conversion and storage: current status and perspectives. Nanoscale, 2018, 10, 11241
[16] Xiao P, Chen W, Wang X. A review of phosphide-based materials for electrocatalytic hydrogen evolution. Adv Energy Mater, 2015, 5, 1500985
[17] Jiao Y, Zheng Y, Jaroniec M, et al. Design of electrocatalysts for oxygen- and hydrogen-involving energy conversion reactions. Chem Soc Rev, 2015, 44, 2060
[18] Zheng Y, Jiao Y, Jaroniec M, et al. Advancing the electrochemistry of the hydrogen-evolution reaction through combining experiment. Angew Chem Int Ed, 2015, 54, 52
[19] Nørskov J K, Bligaard T, Logadottir A, et al. Trends in the exchange current for hydrogen evolution. J Electrochem Soc, 2005, 152, 23
[20] Cook T R, Dogutan D K, Reece S Y, et al. Solar energy supply and storage for the legacy and nonlegacy worlds. Chem Rev, 2010, 110, 6474
[21] Dau H, Limberg C, Reier T, et al. The mechanism of water oxidation: from electrolysis via homogeneous to biological catalysis. ChemCatChem, 2010, 2, 724
[22] Wu L K, Wu W Y, Xia J, et al. A nanostructured nickel-cobalt alloy with an oxide layer for an efficient oxygen evolution reaction. J Mater Chem A, 2017, 5, 10669
[23] Liu K, Zhang C, Sun Y, et al. High-performance transition metal phosphide alloy catalyst for oxygen evolution reaction. ACS Nano, 2018, 12, 158
[24] Liang C, Zou P, Nairan A, et al. Exceptional performance of hierarchical Ni-Fe oxyhydroxide@NiFe alloy nanowire array electrocatalyst for large current density water splitting. Energy Environ Sci, 2020, 13, 86
[25] Mccrory C C L, Jung S, Peters J C, et al. Benchmarking heterogeneous electrocatalysts for the oxygen evolution reaction. J Am Chem Soc, 2013, 135, 16977
[26] Tang C, Wang H F, Zhu X L, et al. Advances in hybrid electrocatalysts for oxygen evolution reactions: Rational integration of NiFe layered double hydroxides and nanocarbon. Part Part Syst Charact, 2016, 33, 473
[27] Man I C, Su H Y, Calle-Vallejo F, et al. Universality in oxygen evolution electrocatalysis on oxide surfaces. ChemCatChem, 2011, 3, 1159
[28] Qazi U Y, Yuan C Z, Ullah N, et al. One-step growth of iron-nickel bimetallic nanoparticles on FeNi alloy foils: Highly efficient advanced electrodes for the oxygen evolution reaction. ACS Appl Mater Interfaces, 2017, 9, 28627
[29] Hu Q, Liu X, Zhu B, et al. Crafting MoC_2-doped bimetallic alloy nanoparticles encapsulated within N-doped graphene as roust bifunctional electrocatalysts for overall water splitting. Nano Energy, 2018, 50, 212
[30] Fan J, Chen Z, Shi H, et al. In situ grown, self-supported iron-cobalt-nickel alloy amorphous oxide nanosheets with low overpotential toward water oxidation. Chem Commun, 2016, 52, 4290
[31] Jin Y, Yue X, Shu C, et al. Three-dimensional porous $MoNi_4$ networks constructed by nanosheets as bifunctional electrocatalysts for overall water splitting. J Mater Chem A, 2017, 5, 2508
[32] Ma Y, Dai X, Liu M, et al. Strongly coupled feni alloys/$NiFe_2O_4$@carbonitride layers-assembled microboxes for enhanced oxygen evolution reaction. ACS Appl Mater Interfaces, 2016, 8, 34396
[33] Chung D Y, Lopes P P, Martins P F, et al. Dynamic stability of active sites in hydr(oxy)oxides for the oxygen evolution reaction. Nat Energy, 2020, 5, 222
[34] Saha S, Ganguli A K. FeCoNi alloy as noble metal-free electrocatalyst for oxygen evolution reaction (OER). ChemistrySelect, 2017, 2, 1630
[35] Zhang P, Li L, Nordlund D, et al. Dendritic core-shell nickel-iron-copper metal/metal oxide electrode for efficient electrocatalytic water oxidation. Nat Commun, 2018, 9, 381
[36] Zhang J, Shao Q, Wang P, et al. Catalytic hydrogen production by janus CuAg nanostructures. ChemNanoMat, 2018, 4, 477
[37] Song Q, Xue Z, Liu C, et al. A general strategy to optimize gas evolution reaction via assembled striped-pattern superlattices. J Am Chem Soc, 2019, 142, 1857
[38] Garcés-Pineda F A, Blasco-Ahicart M, Nieto-Castro D, et al. Direct magnetic enhancement of electrocatalytic water oxidation in alkaline media. Nat Energy, 2019, 4, 519
[39] Ganesan P, Sivanantham A, Shanmugam S. Nanostructured nickel-cobalt-titanium alloy grown on titanium substrate as efficient electrocatalyst for alkaline water electrolysis. ACS Appl Mater Interfaces, 2017, 9, 12416
[40] Zhu X, Jin T, Tian C, et al. In situ coupling strategy for the preparation of FeCo alloys and Co_4N hybrid for highly efficient oxygen evolution. Adv Mater, 2017, 29, 1704091
[41] Subbaraman R, Tripkovic D, Chang K C, et al. Trends in activity for the water electrolyser reactions on 3d M(Ni,Co,Fe,Mn) hydr(oxy)oxide catalysts. Nat Mater, 2012, 11, 550
[42] Wang F, Kusada K, Wu D, et al. Solid-solution alloy nanoparticles of the immiscible iridium–copper system with a wide composition range for enhanced electrocatalytic applications. Angew Chem Int Ed, 2018, 57, 4505
[43] Zhao Y, Luo M, Chu S, et al. 3D nanoporous iridium-based alloy microwires for efficient oxygen evolution in acidic media. Nano Energy, 2019, 59, 146
[44] Gupta S, Qiao L, Zhao S, et al. Highly active and stable graphene tubes decorated with FeCoNi alloy nanoparticles via a template-free graphitization for bifunctional oxygen reduction and evolution. Adv Energy Mater, 2016, 6, 1601198
[45] Cui X, Ren P, Deng D, et al. Single layer graphene encapsulating non-precious metals as high-performance electrocatalysts for water oxidation. Energy Environ Sci, 2016, 9, 123
[46] Yang Y, Lin Z, Gao S, et al. Tuning electronic structures of nonprecious ternary alloys encapsulated in graphene layers for optimizing overall water splitting activity. ACS Catal, 2017, 7, 469
[47] Wang C, Yang H, Zhang Y, et al. NiFe alloy nanoparticles with hcp crystal structure stimulate superior oxygen evolution reaction electrocatalytic activity. Angew Chem Int Ed, 2019, 58, 6099
[48] Anantharaj S, Karthick K, Venkatesh M, et al. Enhancing electrocatalytic total water splitting at few layer Pt-NiFe layered double hydroxide interfaces. Nano Energy, 2017, 39, 30
[49] Xiang Q, Li F, Chen W, et al. In situ vertical growth of Fe-Ni layered double-hydroxide arrays on Fe-Ni alloy foil: Interfacial layer enhanced electrocatalyst with small overpotential for oxygen evolution reaction. ACS Energy Lett, 2018, 3, 2357
[50] Ge X, Chen L, Zhang L, et al. Nanoporous metal enhanced catalytic activities of amorphous molybdenum sulfide for high-efficiency hydrogen production. Adv Mater, 2014, 26, 3100
[51] Fester J, Makoveev A, Grumelli D, et al. The structure of the cobalt oxide/au catalyst interface in electrochemical water splitting. Angew Chem, 2018, 130, 12069
[52] Ng J W D, García-Melchor M, Bajdich M, et al. Gold-supported cerium-doped NiO_x catalysts for water oxidation. Nat Energy, 2016, 1, 16053
[53] Chakthranont P, Kibsgaard J, Gallo A, et al. Effects of gold substrates on the intrinsic and extrinsic activity of high-loading nickel-based oxyhydroxide oxygen evolution catalysts. ACS Catal, 2017, 7, 5399
[54] Zhao S, Jin R, Abroshan H, et al. Gold nanoclusters promote electrocatalytic water oxidation at the nanocluster/$CoSe_2$ Interface. J Am Chem Soc, 2017, 139, 1077
[55] Gorlin Y, Chung C J, Benck J D, et al. Understanding interactions between manganese oxide and gold that lead to enhanced activity for electrocatalytic water oxidation. J Am Chem Soc, 2014, 136, 4920
[56] Ci S, Mao S, Hou Y, et al. Rational design of mesoporous NiFe-

alloy-based hybrids for oxygen conversion electrocatalysis. J Mater Chem A, 2015, 3, 7986
[57] Wen L, Wang Z, Mi Y, et al. Designing heterogeneous 1D nanostructure arrays based on AAO templates for energy applications. Small, 2015, 11, 3408
[58] Wen L, Xu R, Cui C, et al. Template-guided programmable janus heteronanostructure arrays for efficient plasmonic photocatalysis. Nano Lett, 2018, 18, 4914
[59] Kang J, Hirata A, Qiu H J, et al. Self-grown oxy-hydroxide@nanoporous metal electrode for high-performance supercapacitors. Adv Mater, 2014, 26, 269
[60] Yu L, Zhou H, Sun J, et al. Cu nanowires shelled with NiFe layered double hydroxide nanosheets as bifunctional electrocatalysts for overall water splitting. Energy Environ Sci, 2017, 10, 1820
[61] Zhu X, Amal R, Lu X. N,P co-coordinated manganese atoms in mesoporous carbon for electrochemical oxygen reduction. Small, 2019, 15, 1804524
[62] Zhu X, Tan X, Wu K H, et al. N,P co-coordinated Fe species embedded in carbon hollow spheres for oxygen electrocatalysis. J Mater Chem A, 2019, 7, 14732
[63] Dang Y, He J, Wu T, et al. Constructing bifunctional 3D holey and ultrathin CoP nanosheets for efficient overall water splitting. ACS Appl Mater Interfaces, 2019, 11, 29879
[64] Li M, Liu T, Bo X, et al. A novel flower-like architecture of FeCo@NC-functionalized ultra-thin carbon nanosheets as a highly efficient 3D bifunctional electrocatalyst for full water splitting. J Mater Chem A, 2017, 5, 5413
[65] Zhu X, Zhang D, Chen C J, et al. Harnessing the interplay of Fe–Ni atom pairs embedded in nitrogen-doped carbon for bifunctional oxygen electrocatalysis. Nano Energy, 2020, 71, 104597
[66] Jin J, Yu J, Guo D, et al. A hierarchical Z-scheme CdS-WO_3 photocatalyst with enhanced CO_2 reduction activity. Small, 2015, 11, 5262
[67] Bandarenka A S, Varela AS, Karamad M, et al. Design of an active site towards optimal electrocatalysis: Overlayers, surface alloys and near-surface alloys of Cu/Pt(111). Angew Chem Int Ed, 2012, 51, 11845
[68] Faber M S, Dziedzic R, Lukowski M A, et al. High-performance electrocatalysis using metallic cobalt pyrite (CoS_2) micro- and nanostructures. J Am Chem Soc, 2014, 136, 10053
[69] Huang C L, Chuah X F, Hsieh C T, et al. NiFe alloy nanotube arrays as highly efficient bifunctional electrocatalysts for overall water splitting at high current densities. ACS Appl Mater Interfaces, 2019, 11, 24096
[70] Xu H, Shi Z X, Tong Y X, et al. Porous microrod arrays constructed by carbon-confined NiCo@$NiCoO_2$ core@shell nanoparticles as efficient electrocatalysts for oxygen evolution. Adv Mater, 2018, 30, 1705442
[71] Hou Y, Cui S, Wen Z, et al. Strongly coupled 3D hybrids of n-doped porous carbon nanosheet/CoNi alloy-encapsulated carbon nanotubes for enhanced electrocatalysis. Small, 2015, 11, 5940
[72] Zhang X, Zhao Y F, Zhao Y X, et al. A simple synthetic strategy toward defect-rich porous monolayer NiFe-layered double hydroxide nanosheets for efficient electrocatalytic water oxidation. Adv Energy Mater, 2019, 9, 1900881
[73] Popczun E J, McKone J R, Read C G, et al. Nanostructured nickel phosphide as an electrocatalyst for the hydrogen evolution reaction. J Am Chem Soc, 2013, 135, 9267
[74] Gao M, Sheng W, Zhuang Z, et al. Efficient water oxidation using nanostructured α-nickel-hydroxide as an electrocatalyst. J Am Chem Soc, 2014, 136, 7077
[75] Kim S, Ahn C, Cho Y, et al. Suppressing buoyant force: New avenue for long-term durability of oxygen evolution catalysts. Nano Energy, 2018, 54, 184
[76] Kuhl K P, Cave E R, Abram D N, et al. New insights into the electrochemical reduction of carbon dioxide on metallic copper surfaces. Energy Environ Sci, 2012, 5, 7050
[77] Yang H Z, Shang L, Zhang Q H, et al. A universal ligand mediated method for large scale synthesis of transition metal single atom catalysts. Nat Commun, 2019, 10, 4585
[78] Wang W, Shang L, Chang G J, et al. Intrinsic carbon-defect-driven electrocatalytic reduction of carbon dioxide. Adv Mater, 2019, 31, 1808276
[79] Yoo J S, Christensen R, Vegge T, et al. Theoretical Insight into the trends that guide the electrochemical reduction of carbon dioxide to formic acid. ChemSusChem, 2016, 9, 358
[80] Bagger A, Ju W, Varela A S, et al. Electrochemical CO_2 reduction: A classification problem. ChemPhysChem, 2017, 18, 3266
[81] Peterson A A, Nørskov J K. Activity descriptors for CO_2 electroreduction to methane on transition-metal catalysts. J Phys Chem Lett, 2012, 3, 251
[82] Kuhl K P, Hatsukade T, Cave E R, et al. Electrocatalytic conversion of carbon dioxide to methane and methanol on transition metal surfaces. J Am Chem Soc, 2014, 136, 14107
[83] Peterson A A, Abild-Pedersen F, Studt F, et al. How copper catalyzes the electroreduction of carbon dioxide into hydrocarbon fuels. Energy Environ Sci, 2010, 3, 1311
[84] Ooka H, Figueiredo M C, Koper M T M. Competition between hydrogen evolution and carbon dioxide reduction on copper electrodes in mildly acidic media. Langmuir, 2017, 33, 9307
[85] He J, Johnson N J J, Huang A, et al. Electrocatalytic alloys for CO_2 reduction. ChemSusChem, 2018, 11, 48
[86] Chen D, Wang Y L, Liu D Y, et al. Surface composition dominates the electrocatalytic reduction of CO_2 on ultrafine CuPd nanoalloys. Carbon Energy, 2020, 2, 443
[87] Schouten K J P, Kwon Y, Van Der Ham C J M, et al. A new mechanism for the selectivity to C_1 and C_2 species in the electrochemical reduction of carbon dioxide on copper electrodes. Chem Sci, 2011, 2, 1902
[88] Hori Y, Takahashi R, Yoshinami Y, et al. Electrochemical reduction of CO at a copper electrode. J Phys Chem B, 1997, 101, 7075
[89] Cook R L, Macduff R C, Sammells A F. Evidence for formaldehyde, formic acid, and acetaldehyde as possible intermediates during electrochemical carbon dioxide reduction at copper. J Electrochem Soc, 1989, 136, 1982
[90] Montoya J H, Shi C, Chan K, et al. Theoretical insights into a CO dimerization mechanism in CO_2 electroreduction. J Phys Chem Lett, 2015, 6, 2032
[91] Schouten K J P, Qin Z, Gallent E P, et al. Two pathways for the formation of ethylene in CO reduction on single-crystal copper electrodes. J Am Chem Soc, 2012, 134, 9864
[92] Fan Q, Zhang M, Jia M, et al. Electrochemical CO_2 reduction to C_{2+} species: Heterogeneous electrocatalysts, reaction pathways, and optimization strategies. Mater Today Energy, 2018, 10, 280
[93] Calvinho K U D, Laursen A B, Yap K M K, et al. Selective CO_2 reduction to C_3 and C_4 oxyhydrocarbons on nickel phosphides at overpotentials as low as 10 mV. Energy Environ Sci, 2018, 11, 2550
[94] Kortlever R, Peters I, Balemans C, et al. Palladium-gold catalyst for the electrochemical reduction of CO_2 to C1-C5 hydrocarbons. Chem Commun, 2016, 52, 10229
[95] Torelli D A, Francis S A, Crompton J C, et al. Nickel-gallium-catalyzed electrochemical reduction of CO_2 to highly reduced products at low overpotentials. ACS Catal, 2016, 6, 2100
[96] Garza A J, Bell A T, Head-Gordon M. Mechanism of CO_2 reduction at copper surfaces: Pathways to C_2 products. ACS Catal, 2018, 8, 1490
[97] Resasco J, Chen L D, Clark E, et al. Promoter effects of alkali metal cations on the electrochemical reduction of carbon dioxide. J Am Chem Soc, 2017, 139, 11277
[98] Ledezma-Yanez I, Gallent E P, Koper M T M, et al. Structure-sensit-

ive electroreduction of acetaldehyde to ethanol on copper and its mechanistic implications for CO and CO_2 reduction. Catal Today, 2016, 262, 90

[99] Clark E L, Bell A T. Direct observation of the local reaction environment during the electrochemical reduction of CO_2. J Am Chem Soc, 2018, 140, 7012

[100] Kortlever R, Shen J, Schouten K J P, et al. Catalysts and reaction pathways for the electrochemical reduction of carbon dioxide. J Phys Chem Lett, 2015, 6, 4073

[101] Tang W, Peterson A A, Varela A S, et al. The importance of surface morphology in controlling the selectivity of polycrystalline copper for CO_2 electroreduction. Phys Chem Chem Phys, 2012, 14, 76

[102] Loiudice A, Lobaccaro P, Kamali E A, et al. Tailoring copper nanocrystals towards C_2 products in electrochemical CO_2 reduction. Angew Chem, 2016, 128, 5883

[103] Ma M, Trześniewski B J, Xie J, et al. Selective and efficient reduction of carbon dioxide to carbon monoxide on oxide-derived nanostructured silver electrocatalysts. Angew Chem, 2016, 128, 9900

[104] Rosen B A, Salehi-khojin A, Thorson M R, et al. Ionic liquid-mediated selective conversion of CO_2 to CO at low overpotentials. Science, 2011, 334, 643

[105] Liu M, Pang Y, Zhang B, et al. Enhanced electrocatalytic CO_2 reduction via field-induced reagent concentration. Nature, 2016, 537, 382

[106] Asadi M, Kim K, Liu C, et al. Nanostructured transition metal dichalcogenide electrocatalysts for CO_2 reduction in ionic liquid. Science, 2016, 353, 467

[107] Gao S, Lin Y, Jiao X, et al. Partially oxidized atomic cobalt layers for carbon dioxide electroreduction to liquid fuel. Nature, 2016, 529, 68

[108] White J L, Baruch M F, Pander J E, et al. Light-driven heterogeneous reduction of carbon dioxide: Photocatalysts and photoelectrodes. Chem Rev, 2015, 115, 12888

[109] Choi S Y, Jeong S K, Kim H J, et al. Electrochemical reduction of carbon dioxide to formate on tin-lead alloys. ACS Sustain Chem Eng, 2016, 4, 1311

[110] Lee C H, Kanan M W. Controlling H^+ vs CO_2 reduction selectivity on Pb electrodes. ACS Catal, 2015, 5, 465

[111] MacHunda R L, Ju H, Lee J. Electrocatalytic reduction of CO_2 gas at Sn based gas diffusion electrode. Curr Appl Phys, 2011, 11, 986

[112] Luc W, Collins C, Wang S, et al. Ag-Sn bimetallic catalyst with a core-shell structure for CO_2 reduction. J Am Chem Soc, 2017, 139, 1885

[113] Bai X, Chen W, Zhao C, et al. Exclusive formation of formic acid from CO_2 electroreduction by a tunable Pd-Sn alloy. Angew Chem Int Ed, 2017, 56, 12219

[114] Kortlever R, Peters I, Koper S, et al. Electrochemical CO_2 reduction to formic acid at low overpotential and with high faradaic efficiency on carbon-supported bimetallic Pd-Pt nanoparticles. ACS Catal, 2015, 5, 3916

[115] Hahn C, Abram D N, Hansen H A, et al. Synthesis of thin film AuPd alloys and their investigation for electrocatalytic CO_2 reduction. J Mater Chem A, 2015, 3, 20185

[116] Min X, Kanan M W. Pd-catalyzed electrohydrogenation of carbon dioxide to formate: High mass activity at low overpotential and identification of the deactivation pathway. J Am Chem Soc, 2015, 137, 4701

[117] da Silva S G, Silva J C M, Buzzo G S, et al. PdAu/C electrocatalysts as anodes for direct formate fuel cell. Electrocatalysis, 2015, 6, 442

[118] Xu Z, Lai E, Shao-Horn Y, et al. Compositional dependence of the stability of AuCu alloy nanoparticles. Chem Commun, 2012, 48, 5626

[119] Hirunsit P. Electroreduction of carbon dioxide to methane on copper, copper-silver, and copper-gold catalysts: A DFT study. J Phys Chem C, 2013, 117, 8262

[120] Kim D, Resasco J, Yu Y, et al. Synergistic geometric and electronic effects for electrochemical reduction of carbon dioxide using gold-copper bimetallic nanoparticles. Nat Commun, 2014, 5, 4948

[121] Rasul S, Anjum D H, Jedidi A, et al. A highly selective copper-indium bimetallic electrocatalyst for the electrochemical reduction of aqueous CO_2 to CO. Angew Chem, 2015, 127, 2174

[122] Sarfraz S, Garcia-Esparza AT, Jedidi A, et al. Cu-Sn bimetallic catalyst for selective aqueous electroreduction of CO_2 to CO. ACS Catal, 2016, 6, 2842

[123] Li M, Wang J, Li P, et al. Mesoporous palladium-copper bimetallic electrodes for selective electrocatalytic reduction of aqueous CO_2 to CO. J Mater Chem A, 2016, 4, 4776

[124] Yin Z, Gao D, Yao S, et al. Highly selective palladium-copper bimetallic electrocatalysts for the electrochemical reduction of CO_2 to CO. Nano Energy, 2016, 27, 35

[125] Kim D, Xie C, Becknell N, et al. Electrochemical activation of CO_2 through atomic ordering transformations of AuCu nanoparticles. J Am Chem Soc, 2017, 139, 8329

[126] Bernal M, Bagger A, Scholten F, et al. CO_2 electroreduction on copper-cobalt nanoparticles: Size and composition effect. Nano Energy, 2018, 53, 27

[127] Chen D, Yao Q, Cui P, et al. Tailoring the selectivity of bimetallic copper-palladium nanoalloys for electrocatalytic reduction of CO_2 to CO. ACS Appl. Energy Mater, 2018, 1, 883

[128] Hori Y, Takahashi I, Koga O, et al. Selective formation of C_2 compounds from electrochemical reduction of CO_2 at a series of copper single crystal electrodes. J Phys Chem B, 2002, 106, 15

[129] Jia F, Yu X, Zhang L. Enhanced selectivity for the electrochemical reduction of CO_2 to alcohols in aqueous solution with nanostructured Cu-Au alloy as catalyst. J Power Sources, 2014, 252, 85

[130] Guo X, Zhang Y, Deng C, et al. Composition dependent activity of Cu-Pt nanocrystals for electrochemical reduction of CO_2. Chem Commun, 2015, 51, 1345

[131] Ren D, Ang B S H, Yeo B S. Tuning the selectivity of carbon dioxide electroreduction toward ethanol on oxide-derived Cu_xZn catalysts. ACS Catal, 2016, 6, 8239

[132] Clark E L, Hahn C, Jaramillo T F, et al. Electrochemical CO_2 reduction over compressively strained CuAg surface alloys with enhanced multi-carbon oxygenate selectivity. J Am Chem Soc, 2017, 139, 15848

[133] Ma S, Sadakiyo M, Heim M, et al. Electroreduction of carbon dioxide to hydrocarbons using bimetallic Cu-Pd catalysts with different mixing patterns. J Am Chem Soc, 2017, 139, 47

[134] Gao D, Zhang Y, Zhou Z, et al. Enhancing CO_2 electroreduction with the metal-oxide interface. J Am Chem Soc, 2017, 139, 5652

[135] Rogers C, Perkins W S, Veber G, et al. Synergistic enhancement of electrocatalytic CO_2 reduction with gold nanoparticles embedded in functional graphene nanoribbon composite electrodes. J Am Chem Soc, 2017, 139, 4052

[136] Lee S, Park G, Lee J. Importance of Ag-Cu biphasic boundaries for selective electrochemical reduction of CO_2 to ethanol. ACS Catal, 2017, 7, 8594

[137] Huang J, Mensi M, Oveisi E, et al. Structural sensitivities in bimetallic catalysts for electrochemical CO_2 reduction revealed by Ag-Cu nanodimers. J Am Chem Soc, 2019, 141, 2490

[138] Guntern Y T, Pankhurst J R, Vávra J, et al. Nanocrystal/metal–organic framework hybrids as electrocatalytic platforms for CO_2 conversion. Angew Chem Int Ed, 2019, 58, 12632

[139] Yuan J, Yang M P, Zhi W Y, et al. Efficient electrochemical reduction of CO_2 to ethanol on Cu nanoparticles decorated on N-doped graphene oxide catalysts. J CO_2 Util, 2019, 33, 452

[140] Carlos G M, Etosha R C, Stephanie A N, et al. Improved CO_2 reduction activity towards C_{2+} alcohols on a tandem gold on copper electrocatalyst. Nat Catal, 2018, 1, 764

[141] Peter B O, Patrick W, Tania M B, et al. Cascade reaction in nanozymes: spatially separated active sites inside Ag-core-porous-Cu-shell nanoparticles for multistep carbon dioxide reduction to higher organic molecules. J Am Chem Soc, 2019, 141, 36

[142] Wang X L, de Araújo J F, Ju W, et al. Mechanistic reaction pathways of enhanced ethylene yields during electroreduction of CO_2-CO co-feeds on Cu and Cu-tandem electrocatalysts. Nat Nanotechnol, 2019, 14, 1063

[143] Haochen Z, Xiaoxia C, Jingguang G C, et al. Computational and experimental demonstrations of one-pot tandem catalysis for electrochemical carbon dioxide reduction to methane. Nat Commun, 2019, 10, 3340

[144] Varela A S, Schlaup C, Jovanov Z P, et al. CO_2 electroreduction on well-defined bimetallic surfaces: Cu overlayers on Pt(111) and Pt(211). J Phys Chem C, 2013, 117, 20500

[145] Sen S, Liu D, Palmore G T R. Electrochemical reduction of CO_2 at copper nanofoams. ACS Catal, 2014, 4, 3091

[146] Roberts F S, Kuhl K P, Nilsson A. High selectivity for ethylene from carbon dioxide reduction over copper nanocube electrocatalysts. Angew Chem, 2015, 127, 5268

[147] Reske R, Duca M, Oezaslan M, et al. Controlling catalytic selectivities during CO_2 electroreduction on thin Cu metal overlayers. J Phys Chem Lett, 2013, 4, 2410

[148] Wakerley D, Lamaison S, Ozanam F, et al. Bio-inspired hydrophobicity promotes CO_2 reduction on a Cu surface. Nat Mater, 2019, 18, 1222

[149] Liu J, Fu J, Zhou Y, et al. Controlled synthesis of EDTA modified porous hollow copper microspheres for high-efficiency conversion of CO_2 to multi-carbon products. Nano Lett, 2020, 20, 7

[150] Dunwell M, Lu Q, Heyes J M, et al. The central role of bicarbonate in the electrochemical reduction of carbon dioxide on gold. J Am Chem Soc, 2017, 139, 3774

[151] Zhu S, Jiang B, Cai W B, et al. Direct observation on reaction intermediates and the role of bicarbonate anions in CO_2 electrochemical reduction reaction on Cu surfaces. J Am Chem Soc, 2017, 139, 15664

[152] Wuttig A, Yoon Y, Ryu J, et al. Bicarbonate is not a general acid in Au-catalyzed CO_2 electroreduction. J Am Chem Soc, 2017, 139, 17109